PROTEINS
STRUCTURE ■ FUNCTION ■ BIOINFORMATICS

The SCP2-thiolase-like protein (SLP) of *Trypanosoma brucei* is an enzyme involved in lipid metabolism

Rajesh K. Harijan,[1,2] Muriel Mazet,[3,4] Tiila R. Kiema,[1] Guillaume Bouyssou,[5] Stefan E. H. Alexson,[6] Ulrich Bergmann,[1] Patrick Moreau,[5] Paul A. M. Michels,[7] Frédéric Bringaud,[3,4]* and Rik K. Wierenga[1]*

[1] Faculty of Biochemistry and Molecular Medicine, Biocenter Oulu, University of Oulu, Oulu, FIN-90014, Finland

[2] Department of Biochemistry, Albert Einstein College of Medicine, 1300 Morris Park Avenue, Bronx, New York 10461, USA

[3] Centre De Résonance Magnétique Des Systèmes Biologiques (RMSB), UMR5536, Université De Bordeaux, CNRS, 146 Rue Léo Saignat, Bordeaux, 33076, France

[4] Laboratoire De Microbiologie Fondamentale Et Pathogénicité (MFP), UMR5234, , Université De Bordeaux, CNRS, 146 Rue Léo Saignat, Bordeaux, 33076, France

[5] Laboratoire De Biogenèse Membranaire, UMR-5200, Université De Bordeaux, CNRS, Bâtiment A3 - 1er Étage, INRA Bordeaux Aquitaine BP81, 71 Avenue Edouard Bourlaux, Villenave D'Ornon Cedex, 33883, France

[6] Karolinska Institutet, Department of Laboratory Medicine, Division of Clinical Chemistry, Karolinska University Hospital, Stockholm, SE 141 86, Sweden

[7] Centre for Immunity, Infection and Evolution and Centre for Translational and Chemical Biology, School of Biological Sciences, the King's Buildings, University of Edinburgh, Charlotte Auerbach Road, Edinburgh, EH9 3FL, United Kingdom

ABSTRACT

Bioinformatics studies have shown that the genomes of trypanosomatid species each encode one SCP2-thiolase-like protein (SLP), which is characterized by having the YDCF thiolase sequence fingerprint of the Cβ2-Cα2 loop. SLPs are only encoded by the genomes of these parasitic protists and not by those of mammals, including human. Deletion of the *Trypanosoma brucei* SLP gene (TbSLP) increases the doubling time of procyclic *T. brucei* and causes a 5-fold reduction of *de novo* sterol biosynthesis from glucose- and acetate-derived acetyl-CoA. Fluorescence analyses of EGFP-tagged TbSLP expressed in the parasite located the TbSLP in the mitochondrion. The crystal structure of TbSLP (refined at 1.75 Å resolution) confirms that TbSLP has the canonical dimeric thiolase fold. In addition, the structures of the TbSLP-acetoacetyl-CoA (1.90 Å) and TbSLP-malonyl-CoA (2.30 Å) complexes reveal that the two oxyanion holes of the thiolase active site are preserved. TbSLP binds malonyl-CoA tightly (K_d 90 μM), acetoacetyl-CoA moderately (K_d 0.9 m*M*) and acetyl-CoA and CoA very weakly. TbSLP possesses low malonyl-CoA decarboxylase activity. Altogether, the data show that TbSLP is a mitochondrial enzyme involved in lipid metabolism.

Proteins 2016; 84:1075–1096.

Additional Supporting Information may be found in the online version of this article.

Abbreviations: AB-thiolase, dimeric peroxisomal thiolase; ACP, acyl carrier protein; ASCT, mitochondrial acetate:succinate CoA-transferase; CoA, coenzyme A; CT-thiolase, tetrameric cytosolic thiolase; β-ME, β-mercaptoethanol; EGFP, enhanced green fluorescent protein; FAME, fatty acid methyl ester; FAS, fatty acid synthesis; HAD, medium chain L-3-hydroxyacyl-CoA dehydrogenase; HPLC, high performance liquid chromatography; HPTLC, high performance thin layer chromatography; KAS, 3-ketoacyl ACP synthase; Lm-thiolase, dimeric *Leishmania mexicana* SCP2-thiolase (type-2); MCAT, malonyl-CoA:ACP transacylase; OAH, oxyanion hole; PEG, polyethylene glycol; Sc-thiolase, *Saccharomyces cerevisiae* AB-thiolase; SCP2-thiolase, mammalian dimeric peroxisomal SCP2-thiolase (type-1); SLP, SCP2-thiolase like protein; SLS, static light scattering; SPR, surface plasmon resonance; Tb-thiolase, dimeric *T. b. brucei* SCP2-thiolase (type-2); TbSLP, SCP2-thiolase like protein of *T. b. brucei*; TDH, threonine dehydrogenase; T1-thiolase, tetrameric mitochondrial medium chain T1-thiolase; T2-thiolase, tetrameric mitochondrial short chain T2-thiolase; TFE-thiolase, dimeric mitochondrial trifunctional enzyme thiolase; Tris, 2-amino-2-hydroxymethyl-propane-1,3-diol; Zr-thiolase, bacterial tetrameric *Zoogloea ramigera* CT-thiolase

Grant sponsor: Academy of Finland (to R.K.W.); Grant number: 131795; Grant sponsor: European Community's Seventh Framework Programme [(FP7/2007–2013) under BioStruct-X]; Grant number: 283570; Grant sponsor: Ville Ratas (technical support) and Academy of Finland (xtalPiMS project; 141487); Grant sponsor: Centre National de la Recherche Scientifique (CNRS), the Université de Bordeaux, the Agence Nationale de la Recherche [(ANR) ACETOTRYP of the ANR-BLANC-2010 and the Laboratoire d'Excellence (LabEx) ParaFrap ANR-11-LABX-0024].

Rajesh K. Harijan and Muriel Mazet contributed equally to this work.

*Correspondence to: Rik K. Wierenga; Faculty of Biochemistry and Molecular Medicine, Biocenter Oulu, University of Oulu, Oulu, Finland FIN-90014. E-mail: rik.wierenga@oulu.fi or Frédéric Bringaud; Parasitologie Moléculaire et Pathogénicité, UMR5234 CNRS, UMR5536, Université de Bordeaux, CNRS, 146 rue Léo Saignat, 33076 Bordeaux, France. E-mail: frederic.bringaud@u-bordeaux.fr

Received 1 November 2015; Revised 3 April 2016; Accepted 8 April 2016
Published online 19 April 2016 in Wiley Online Library (wileyonlinelibrary.com). DOI: 10.1002/prot.25054

Key words: Trypanosoma brucei; SCP2-thiolase; SCP2-thiolase-like protein; malonyl-CoA decarboxylase; malonyl-CoA:ACP transacylase; gene knockout; crystal structure; mitochondrial lipid metabolism.

INTRODUCTION

A recent bioinformatics study of 130 thiolase sequences identified two families of thiolase-like proteins, of which the sequences have significant sequence similarity to thiolase enzymes, but nevertheless key catalytic residues, including the nucleophilic cysteine, are not conserved.[1] These thiolase-like sequences are referred to as TLPs (thiolase-like proteins) and SLPs (SCP2-thiolase-like proteins), respectively. TLPs were only found in the genomes of mycobacteria. A crystal structure of the monomeric TLP from *Mycobacterium smegmatis* has been reported, confirming its thiolase fold, however the function of TLPs is still unknown.[2] The structure and the function of the SLPs are not known, and these topics are addressed in the studies reported here.

Thiolases form a subfamily of enzymes that belong to the thiolase superfamily. This superfamily comprises enzymes involved in lipid metabolism, known to be involved in the degradation of lipids, like the degradative thiolases, as well as in lipid biosynthesis, for example, the KAS enzymes (3-ketoacyl-ACP-synthases).[3] The degradative thiolases catalyze the thiolytic cleavage of 3-ketoacyl moieties, whereas the KAS enzymes catalyze the reverse reaction, being a Claisen condensation reaction in which a C—C bond is formed. The fatty acid substrates of the thiolase superfamily enzymes are conjugated via a thioester bond to either the pantetheine moiety of CoA, for example, in the case of thiolase, or to the phosphopantetheine moiety of ACP (acyl carrier protein), as in the case of KAS enzymes. ACP is a small helical protein to which the phosphopantetheine group is covalently bound to a conserved serine, via a phosphate ester bond and this covalent complex is important in the fatty acid synthesis (FAS) pathway.[4] The reactive thioester bond in the conjugated fatty acids facilitates further metabolic conversions. The thiolase superfamily also includes other CoA and ACP dependent enzymes like chalcone synthase, the polyketide synthases (PKS enzymes),[5] and HMG-CoA synthase,[6–8] all of which catalyze a Claisen condensation reaction. In this synthetic reaction, two mechanisms are used to generate the reactive nucleophile, either by deprotonation (such as in the well-studied biosynthetic CT-thiolase of *Zoogloea ramigera*) or by decarboxylation (such as in the KAS enzymes and in chalcone synthase). In the latter case, the substrate is either malonyl-ACP (in case of KAS enzymes) or malonyl-CoA (in case of chalcone synthase). The thiolase superfamily enzymes are characterized by having active sites with two oxyanion holes (OAHs) (Fig. 1), which are formed by conserved sequence motifs (Fig. 2). Metal ions or other cofactors are not required for catalysis by the enzymes of this superfamily.

The enzymes of the thiolase subfamily are oligomers of approximately 40 kDa polypeptide chains that are assembled as tight dimers or tetramers, being dimers of tight dimers. Six human thiolases have been identified, including three tetrameric enzymes, T1-, T2,- and CT-thiolases, and three dimeric enzymes, AB-, TFE-, and SCP2-thiolases.[1] Structures of the human tetrameric CT-thiolase,[9] T1-thiolase[10] and T2-thiolase[11] are known. Structures have been described for the degradative dimeric peroxisomal AB-thiolase of human (PDB accession code: 2IIK), yeast,[12] and plant,[13] as well as for two bacterial dimeric, degradative TFE-thiolases.[14,15] The mammalian peroxisomal SCP2-thiolase (also known as the SCP2-thiolase [type-1])[1] has an extra domain, the SCP2 domain. This domain (approximately 130 residues) binds lipids and it is located at its C-terminus. The structure of this SCP2-thiolase has not yet been reported, but the crystal structure of the trypanosomal SCP2-thiolase (not having the SCP2 domain), also known as the type-2 SCP2-thiolase, has been published recently.[16]

The thiolase fold consists of three domains, each of approximately 120 residues, the N-terminal domain, the loop domain and the C-terminal domain (Fig. 2). The N- and C-terminal domains share the same βαβαβαββ topology, and both domains provide catalytic residues. The loop domain is important for binding the CoA-moiety, and it occurs as an insertion in the N-terminal domain.[3] The pantetheine binding tunnel is shaped by the Lα1-helix present in the beginning of the loop domain and the pantetheine loop, located at the end of the loop domain. The tetramerization and cationic loops of the loop domain are important for the assembly and function of the tetrameric thiolases. Five active site loops, being part of either the N-terminal domain or the C-terminal domain, and having specific sequence fingerprints, have been identified (Figs. 1 and 2).

In *Z. ramigera* thiolase, closely related to the mammalian CT-thiolase, the Cβ2-Cα2 loop has the NEAF sequence fingerprint (Fig. 2).[17] The CxS loop (also known as the Nβ3-Nα3 loop) is another important loop providing the nucleophilic cysteine (Fig. 1). The other three active site loops (labeled in Fig. 2) are the Cβ3-Cα3 loop (with the GHP motif, providing a catalytic histidine to activate the nucleophilic cysteine) and the Cβ4-Cβ5 loop with the CxG motif, providing the cysteine as the catalytic base. Finally, the Cβ1-Cα1 VMG-motif (Fig. 2) correlates with active sites in which a 2-methyl group of the acyl-chain does not bind. An important feature of

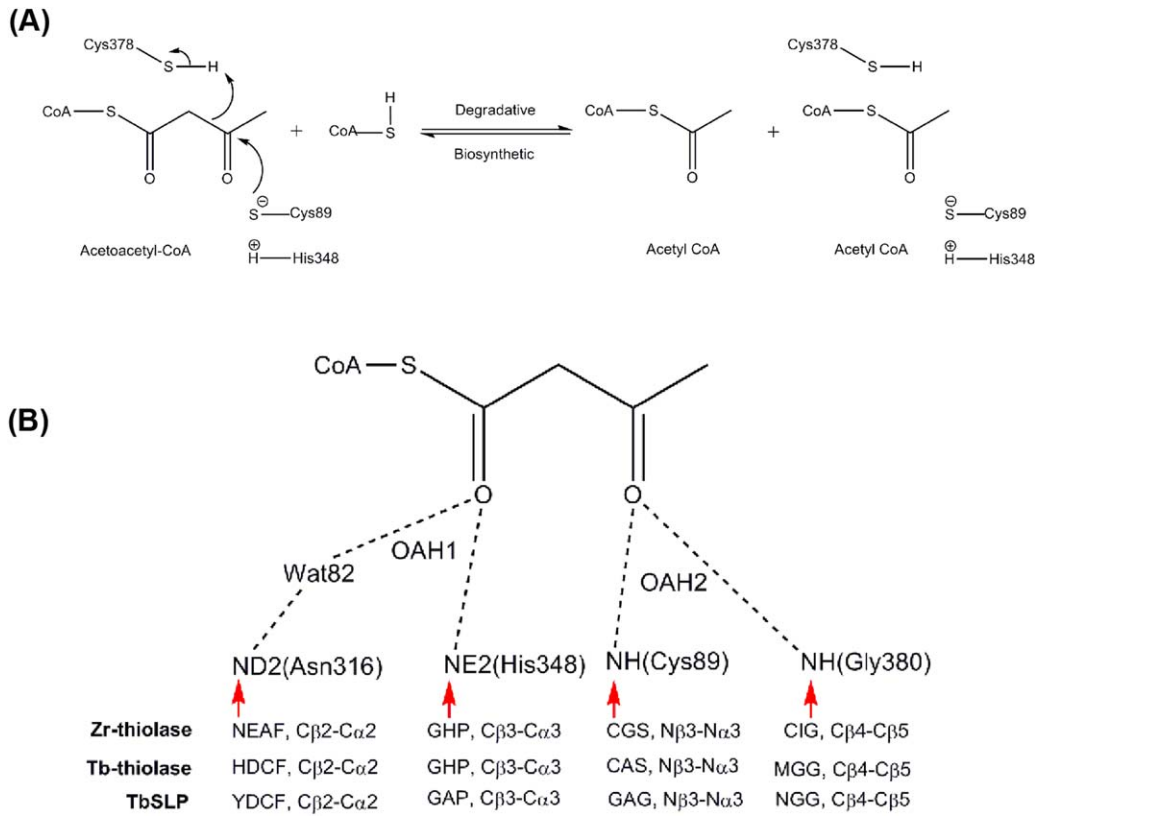

Figure 1

The reaction catalyzed by a thiolase. **A.** Visualized, from left to right, is the overall reaction in the degradative direction. The residue numbering refers to the *Z. ramigera* CT-thiolase. **B.** The oxyanion hole (OAH) hydrogen bond interactions of thiolases for OAH1 and OAH2. The sequence fingerprints of the *Z. ramigera* CT-thiolase (Zr-thiolase), the *T. brucei* SCP2-thiolase, type-2 (Tb-thiolase), and the *T. brucei* SLP (TbSLP) are shown. [Color figure can be viewed in the online issue, which is available at wileyonlinelibrary.com.]

the thiolase catalytic site is the presence of two OAHs, which facilitate the catalysis. OAH1 (formed by a water dyad with the NEAF-asparagine and the GHP-histidine) binds the acyl-CoA thioester oxygen atom and OAH2 (formed by main chain NH-groups of the CxS-loop and the CxG-loop) binds the thioester oxygen of the acylated cysteine (Fig. 1).

Bioinformatics studies revealed that TLPs and SLPs are subfamilies of the SCP2-thiolase set of enzymes showing a unique Cβ2-Cα2 fingerprint sequence, that is, YSCF and YDCF, respectively, instead of NEAF, HEAF or HDCF present in *bona fide* thiolases.[1] SLPs were only found in a group of unicellular eukaryotic parasites, named trypanosomatids, which includes members responsible for serious diseases in humans as well as in other mammals, especially in the tropical and subtropical regions of Latin America, Asia, and Africa. These diseases, caused by several species of *Leishmania* (leishmaniasis), *Trypanosoma brucei* (sleeping sickness) and *Trypanosoma cruzi* (Chagas disease), have been classified by the World Health Organisation (WHO) as neglected tropical diseases. In 2011, the WHO reported two million new cases of trypanosomatid infections.[18] These parasites are transmitted between mammalian hosts by insects such as the tsetse fly, the vector responsible for transmission of *T. brucei*. The major *T. brucei* forms studied *in vitro* are the procyclic form living in the tsetse fly's midgut, and the bloodstream forms of the mammalian host. The natural environments encountered by the mammalian and insect forms of *T. brucei* are so different that important metabolic differences exist between these life-cycle stages to optimize their proliferation in the respective hosts. Anyway, lipid metabolism, which is under investigation here, is essential for growth and development of both the trypanosomal procyclic and bloodstream forms.[19,20]

Here, we report on the detailed structural, biophysical and *in vivo* characterization of the SCP2-thiolase-like protein from *T. brucei* (TbSLP). The structural study confirms that TbSLP is a dimeric protein and each subunit has the characteristic thiolase fold. Cell biological studies show that TbSLP is located in the mitochondrion where it appears to be involved in lipid metabolism.

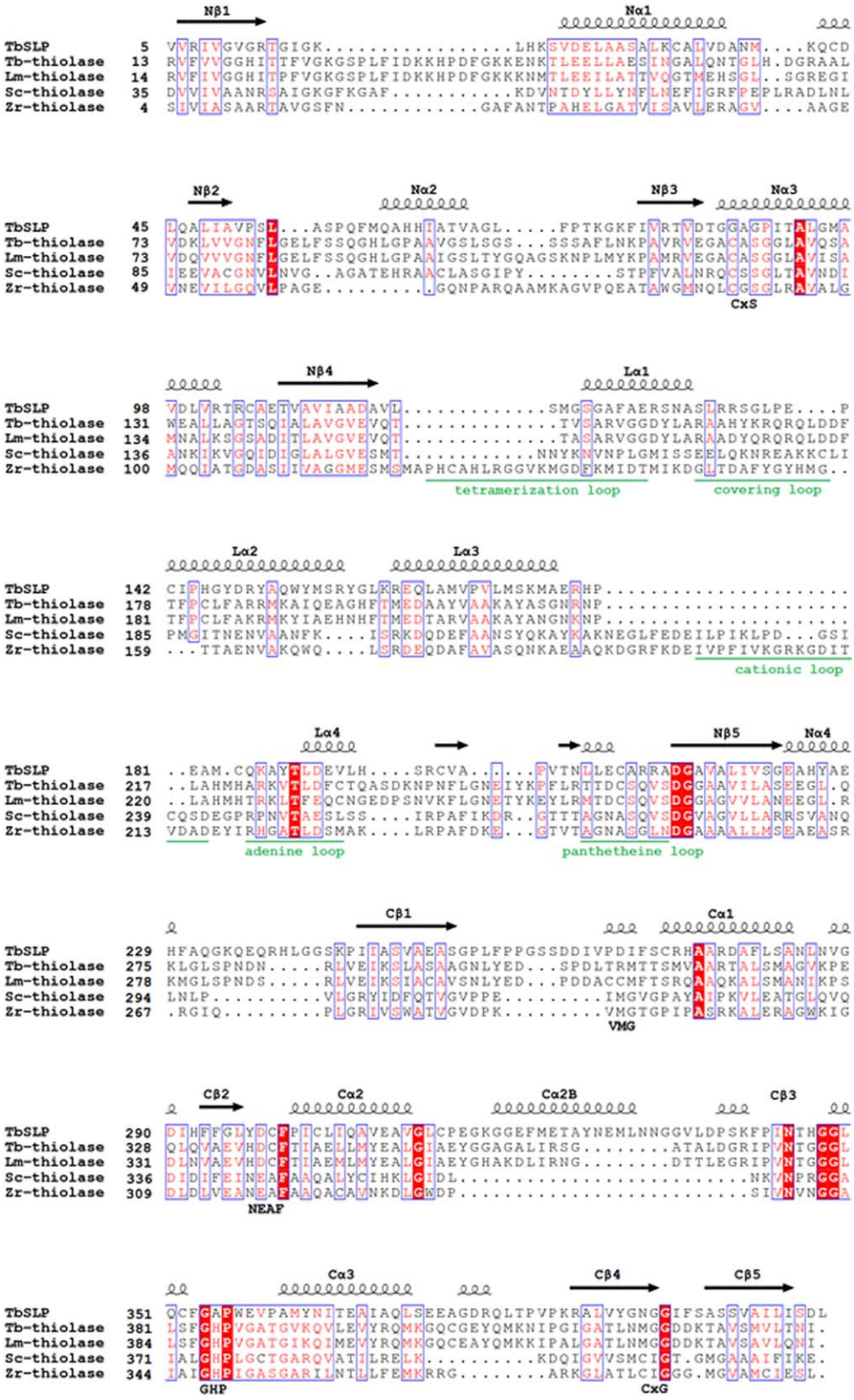

Figure 2

Structure-based sequence alignment of TbSLP with SCP2-thiolase from *T. brucei* (Tb-thiolase, 4BI9) and *L. mexicana* (Lm-thiolase, 3ZBG), *S. cerevisiae* AB-thiolase (Sc-thiolase, 1AFW), and *Z. ramigera* CT-thiolase (Zr-thiolase, 1DM3). The secondary structure elements of TbSLP are shown above the alignment. Black coils represent helices and black arrows represent β-strands. The five different loops of the loop domain, each having a specific function, are underlined and labeled as follows: tetramerization loop, covering loop, cationic loop, adenine loop, pantetheine loop. The five sequence fingerprints of active site loops are highlighted below the sequences. [Color figure can be viewed in the online issue, which is available at wileyonlinelibrary.com.]

MATERIALS AND METHODS

Culturing of trypanosomes

The procyclic form of *T. brucei* EATRO1125.T7T (*TetR-HYG T7RNAPOL-NEO*) was cultured at 27°C in SDM79 medium containing 10% (v/v) heat-inactivated foetal calf serum (FCS) and 25 μg/mL hemin.[21]

Construction of an EGFP-tagged TbSLP, its expression in trypanosomes and fluorescence analyses

Recombinant fragments corresponding to the full-length TbSLP gene (Tb927.8.1820), followed or preceded by the gene of the enhanced green fluorescent protein (*EGFP*) were expressed in procyclic *T. brucei* using the pLew100 vector containing the *EGFP* gene flanked by unique restriction sites, as described previously.[22] The creation of these procyclic cell lines involved inserting PCR fragments corresponding to the full-length TbSLP gene without its stop codon (TbSLP-EGFP) or ATG initiator codon (EGFP-TbSLP) into the XhoI and XbaI restriction sites of the pLew-EGFP1 and pLew-EGFP2 plasmids,[22] to produce the pLew-TbSLP-EGFP1 and pLew-EGFP2-TbSLP plasmids, respectively. Transfection and selection of drug-resistant clones were performed as reported previously[23] in the EATRO1125.T7T parental cell line, which constitutively expresses the T7 RNA polymerase gene and the tetracycline repressor under the control of a T7 RNA polymerase promoter for tetracycline inducible expression.[24] Transfected EATRO1125.T7T cells were selected in SDM79 medium containing hygromycin B (25 μg/mL), neomycin (10 μg/mL) and phleomycin (5 μg/mL). The selected cell lines *TetR-HYG T7RNAPOL-NEO TbSLP::EGFP-BLE* and *TetR-HYG T7RNAPOL-NEO EGFP::TbSLP-BLE* were called TbSLP-EGFP and EGFP-TbSLP, respectively. Expression of the recombinant *EGFP* proteins was induced by addition of 1 μg/mL tetracycline.

For immunofluorescence analyses with anti-sera against acetate:succinate CoA-transferase (ASCT) and threonine dehydrogenase (TDH) as mitochondrial markers, tetracycline-induced TbSLP-EGFP and EGFP-TbSLP cells were fixed with 4% formaldehyde in PBS, permeabilized with 1% Triton X100 and spread on poly-L-lysine coated slides. The slides were then incubated for 45 min in PBS containing 5% BSA, followed by incubation in PBS with 2% BSA and the primary 1:100 diluted rabbit anti-ASCT or anti-TDH antisera.[25] After washing with PBS, the slides were incubated with 2 μg/mL Alexa 594 anti-rabbit IgG conjugate (Molecular Probes). Slides were then washed and mounted in the SlowFade® antifade reagent (Invitrogen). Cells were visualized with a Leica DM5500B microscope and images were captured by an ORCA®-R^2 camera (Hamamatsu) with Leica MM AF Imaging System software (MetaMorph®).

Gene knockout of TbSLP

Replacement of the TbSLP gene by the blasticidin and puromycin resistance markers via homologous recombination was performed with DNA fragments containing the resistance marker gene flanked by TbSLP UTR sequences, as described previously.[26] Briefly, the pGEMt plasmid was used to clone a HpaI DNA fragment containing either the blasticidin or puromycin resistance marker gene preceded by the TbSLP 5'-UTR fragment (758 bp) and followed by the TbSLP 3'-UTR fragment (754 bp). The TbSLP knockout was generated in the EATRO1125.T7T parental cell line. Two clones of transfected cells (*TetR-HYG T7RNAPOL-NEO* Δ*slp::BLA/*Δ*slp::PURO*), called Δ*slp*-B6 and Δ*slp*-D3, were selected in SDM79 medium containing hygromycin B (25 μg/mL), neomycin (10 μg/mL), blasticidin (10 μg/mL), and puromycin (1 μg/mL).

Lipid labelling from D-[^{14}C]-glucose and [^{14}C]-acetate

10^8 cells in the late exponential growth phase were incubated for 16 h in 5 mL of modified SDM79 medium containing 4 m*M* glucose with 25 μCi D-[U-^{14}C]-glucose (300 mCi/mmol) or 4 m*M* glucose, 1 m*M* acetate and 10 μCi of [1-^{14}C]-acetate (55.3 mCi/mmol), before performing lipid extraction as previously described.[25] Cells were checked microscopically for viability several times during the incubation. Subsequently, lipids were extracted with chloroform:methanol (2:1, v/v) for 30 min at room temperature, and then washed three times with 0.9% NaCl. The solvent of the washed lipid extracts was then evaporated and lipids were dissolved in 1 mL of methanol:H_2SO_4 (40:1, v/v). The trans-esterification of the fatty acids of the lipids was done at 80°C for 60 min. After cooling the samples, 400 μL of hexane (99% pure) and 1.5 mL of H_2O were added, and the mixture was homogenized vigorously during 20 sec. The samples were then centrifuged for 5 min at 1000 *g* to separate phases, and the hexane upper phases containing fatty acid methyl esters (FAMEs) and sterols were recovered without contact with the lower phases. FAMEs and sterols were loaded onto high performance thin layer chromatography (HPTLC) plates developed in hexane/ethylether/acetic acid (90:15:2, v/v) and sterols (R_F 0.20) and FAMEs (R_F 0.90) were separated. They were identified by co-migration with known standards. Their radiolabeling was then determined with a STORM 860 (GE Healthcare).

Cloning, expression, and purification

The TbSLP gene was amplified by the PCR method from the genomic DNA using Pfu DNA polymerase (Fermentas) and the primers TbSLP-*Nde*Ipet28 (5'-CAACGA-**CATATG**GCATCTCAGGTTGTGCGCATTGTCG-3') and TbSLP-*Bam*HIpet28 (5'-CTTACG**GGATCC**CTACAAGTC

ACTAATCAAAATGGC-3') containing NdeI and a BamHI sites (underlined), respectively. The PCR products were purified, digested with NdeI and BamHI (Fermentas), ligated into the expression vector pET28a (Novagen) and sequenced at the Biocenter Oulu sequencing facility. The expressed TbSLP included a $(His)_6$-Ser-Ser-Gly-Leu-Val-Pro-Arg-Gly-Ser-His tag at its N-terminus. *Escherichia coli* BL21(DE3) cells containing the pGro7 chaperone plasmid (GroEL and GroES (Takara Bio, Japan)) were transformed with the pET28a-TbSLP plasmid. The co-expression with these chaperones was required to express the TbSLP in its soluble form.

One colony from an overnight grown plate was used to inoculate 50 mL M9ZB medium containing kanamycin (30 μg/mL) and chloramphenicol (34 μg/mL) and cells were grown at 37°C for 6–8 h with shaking (200 rpm). This pre-inoculum was used to inoculate 4 L of M9ZB medium containing L-arabinose (0.3 mg/mL), kanamycin (30 μg/mL), and chloramphenicol (34 μg/mL) and the culture was kept at 37°C for 3–4 h until the OD_{600} reached 0.7 to 1.0. Then, IPTG (0.1 m*M*) was added for the induction of TbSLP expression and the culturing was continued for 8–12 h at 18°C in a shaker operating at 200 rpm. The harvested cells were suspended in lysis buffer [100 m*M* Tris-HCl, 150 m*M* $(NH_4)_2SO_4$, 15% (v/v) glycerol, 10 m*M* β-mercaptoethanol (β-ME), 1% (w/v) Triton X-100, 5.0 m*M* ATP, 25 μg/mL DNase I and 25 μg/mL RNase A and two protease inhibitor cocktail tablets (Roche), pH 7.8]. Cell lysis was achieved by brief sonication and was followed by centrifugation at 30,000 *g* for 30 min at 4°C. The supernatant was mixed with pre-equilibrated Ni-NTA resin (Qiagen) and kept for binding for 2–3 h at 4°C. The mixture was then loaded into an empty column and the resin was washed with 200 mL wash buffer [100 m*M* Tris-HCl, 200 m*M* NaCl, 10% (v/v) glycerol, 10 m*M* β-ME, and 20 m*M* imidazole, pH 7.8] to remove non-specifically bound proteins. TbSLP was then eluted in elution buffer [100 m*M* Tris-HCl, 200 m*M* NaCl, 10% (v/v) glycerol and 10 m*M* β-ME, pH 7.8] containing 300 m*M* imidazole. The eluted protein fraction from the affinity chromatography was concentrated to 2.0 mL using an Amicon centrifugal filter (Millipore) and passed through a desalting PD-10 (GE Healthcare) column using buffer [50 m*M* Tris-HCl, 50 m*M* NaCl, 5% (v/v) glycerol, 1 m*M* EDTA, and 1 m*M* dithiothreitol (DTT), pH 7.8]. Then, the protein sample was loaded on an anion exchange Resource Q column (GE Healthcare), which had already been equilibrated with buffer-A [50 m*M* Tris-HCl, 50 m*M* NaCl, 5% (v/v) glycerol, 1 m*M* EDTA, and 1 m*M* DTT, pH 7.8]. The gradient elution of the protein was done using buffer-B [25 m*M* Tris-HCl, 1*M* NaCl, 5% (v/v) glycerol, 1 m*M* EDTA, and 1 m*M* DTT, pH 7.8]. The eluted protein fractions from the Resource Q column were concentrated to a final volume of 2 mL and then loaded onto a high load Superdex 200 (16/60) preparation grade size-exclusion chromatography column pre-equilibrated with the gel filtration buffer [25 m*M* Tris-HCl, 50 m*M* NaCl, 1 m*M* EDTA, and 1 m*M* DTT, pH 7.8]. The purity of the protein was confirmed by SDS-PAGE. The concentration of protein was determined by absorbance at 280 nm using the calculated molar extinction coefficient (Protparam; http://www.expasy.org/tools/protparam.html). After purification, the protein was used for static light scattering (SLS) measurement, crystallization, and enzyme activity assays, or flash frozen for later use in gel filtration buffer.

Determination of the molecular mass and oligomeric state

Purified TbSLP was analyzed by SLS to confirm its molecular mass and oligomeric state. The SLS flow cell was connected to an ÄKTA purifier (GE Healthcare). TbSLP (~0.1 mg in 200 μL) was loaded onto the Superdex 200 (10/300) GL column attached to the ÄKTA purifier and the SLS profiles were analyzed using the ASTRA program. For this experiment, the protein buffer and SLS running buffer were the same as the protein gel filtration buffer (25 m*M* Tris-HCl, 50 m*M* NaCl, 1 m*M* EDTA, and 1 m*M* DTT, pH 7.8).

Thiolase activity assay of TbSLP

The enzyme activity assays of TbSLP were performed using a JASCO V-660 spectrophotometer. The reaction was initiated by adding the enzyme sample after a stable baseline was obtained. A control measurement was carried out by recording the absorption change in the absence of added enzyme. The change in the absorbance per min was calculated using the JASCO software. Each activity was measured three times using two different batches of purified protein. The concentration of CoA in the respective substrate stock solutions was determined using Ellman's test.[27] The acetyl-CoA and acetoacetyl-CoA were first hydrolyzed with hydroxylamine and then the concentration of free CoA was determined by Ellman's test.

The degradative activity assay of TbSLP was performed at 25°C as described previously[11,16,17] using the Mg^{2+} method. The reaction mixture contained 50 m*M* HEPES, pH 7.8, 25 m*M* $MgCl_2$, 60 μM CoA, and 50 μM acetoacetyl-CoA in a reaction volume of 0.5 mL. The disappearance of the Mg^{2+}-acetoacetyl-CoA complex was recorded at 303 nm after addition of 5.0 μg of TbSLP. The molar extinction coefficient (21,400 M^{-1} cm^1)[17,28] of Mg^{2+}-acetoacetyl-CoA complex was used to calculate its specific activity.

The thiolase assay in the synthetic direction was also done for TbSLP. In this assay, the formation of acetoacetyl-CoA was estimated by the coupled enzyme assay described previously.[11] A linker enzyme (human L-3-hydroxyacyl-CoA dehydrogenase, HAD) was used for reducing the product of TbSLP in the reaction mixture.

The reaction was initiated by adding 5.0 μg of TbSLP to the reaction cocktail (0.5 mL) containing 50 m*M* HEPES (pH 7.8), 40 m*M* KCl, 0.2 m*M* NADH, 1 unit (U) of HAD enzyme (1 U is the amount of enzyme that converts 1 μmole per min), 0.5 m*M* DTT and 2 m*M* acetyl-CoA. The rate of NADH oxidation was measured at 340 nm at 25°C. The extinction coefficient (6220 M^{-1} cm^{-1}) of NADH was use for the activity calculations.[17]

HPLC analysis of TbSLP incubated with malonyl-CoA

Recombinant TbSLP was incubated at room temperature for 30 min with different concentrations of malonyl-CoA (5–100 μM) in 200 m*M* KCl, 10 m*M* HEPES, pH 7.8, in the presence of 1 m*M* DTT, in a total volume of 100 μL. 20 μL of the incubation mixture were injected onto an HPLC system using a C18-column (Ultrasphere 10 mm × 25 cm) pre-equilibrated with 100% buffer A (100 m*M* ammonium phosphate, pH 4). CoA-esters and CoA were eluted using a linear gradient of 100% buffer A to 100% buffer B (buffer A:acetonitrile, 50:50) for 21 min followed by isocratic flow with 100% buffer B for 15 min. The elution peaks of CoA-esters and coenzyme A were detected by an UV-detector at 260 nm and analyzed using Chromelion software (Dionex, Thermo Fisher Scientific). The remaining substrates and formed products were quantified by peak area integration using standard curves for malonyl-CoA, acetyl-CoA, and CoA. The kinetic constants were calculated using the GraphPad Prism software based on two experiments. The k_{cat} was calculated assuming a subunit molecular weight of 43 439 for TbSLP.

Surface plasmon resonance

Surface plasmon resonance (SPR) analysis was done using a Biacore T200 (GE Healthcare) to estimate the binding affinities of TbSLP for CoA, acetyl-CoA, acetoacetyl-CoA, and malonyl-CoA. The GE Healthcare standard immobilization protocol (amine coupling method) was used to immobilize TbSLP (50 μg/mL) on a CM5 sensor chip to 12,600 response units (RU). Different concentrations of the ligands (2.0 μM to 6.0 m*M*) were run over the SPR containing sensor chip using as running buffer 50 m*M* phosphate, 150 m*M* NaCl, pH 7.8. The binding and dissociation rates were measured with a flow rate of 20 μL/min. The injection of the ligands was done for three min followed by a flow with ligand-free buffer to analyze the dissociation for 15 min. Curves were corrected for non-specific ligand binding by subtracting the signal obtained for the negative control flow cell. The dissociation constants were derived from a simple 1:1 interaction model using the Biacore data evaluation software.

Mass spectrometry

The product formed during the incubation of TbSLP with acetoacetyl-CoA (from the spectrophotometric assay) and malonyl-CoA was analyzed by matrix assisted laser desorption time of flight (MALDI-TOF) mass spectrometry on an ultrafleXtreme™ instrument (Bruker). Negative ions were recorded in reflectron mode using 2,5-dihydroxybenzoic acid as matrix. Several control samples, for example, reaction mixture without TbSLP, substrate CoA, acetyl-CoA, acetoacetyl-CoA, and malonyl-CoA as well as only assay buffer were analyzed by MALDI-TOF before the real incubation mixtures were measured.

In the acetoacetyl-CoA incubation assay, a reaction mixture of 100 μL (50 m*M* HEPES, pH 7.8, 2 m*M* acetoacetyl-CoA, 2 m*M* CoA) with 10 μg of TbSLP was incubated for 2 h at room temperature and analyzed.

To study malonyl-CoA decarboxylase activity, the reaction mixture of 100 μL (10 m*M* HEPES, pH 7.8, 200 m*M* KCl, 50 μM malonyl-CoA) with 10 μg TbSLP was incubated for 10, 30 and 60 min at room temperature and analyzed by MALDI-TOF mass spectrometry.

Crystallization

The crystallization experiments of TbSLP were done by the sitting drop vapor diffusion method at 22°C using the Hampton (Crystal screen I & II), Molecular Dimension (Proplex, JCSG and PACT) and homemade factorial crystallization conditions.[29] The drops were set up in 96 well Corning plates using Freedom EVO-100 crystallization robot (TECAN). Each crystallization drop contained 1.5 μL of protein solution (5 mg/mL in gel filtration buffer) and 1.5 μL of well solution. The volume of the well solution was 80 μL. The crystallization plates were placed in a Formulatrix imager and the results were monitored using the in-house xtalPiMS software. The crystals grew in about 5–7 days. Apo TbSLP was crystallized in two different crystallization conditions, being 100 m*M* sodium citrate, pH 5.5, 10% (w/v) PEG4000, 200 m*M* sodium acetate (form-I) and 100 m*M* sodium acetate, pH 4.6, 2.0 M ammonium sulphate (form-II) (Table I).

Data collection, data processing, structure determination, and refinement

The high resolution data set of apo TbSLP was collected using a form-I crystal, after being cryoprotected by transferring it to a mother liquor with 25% PEG4000 (Table I). The X-ray diffraction data of this crystal were collected at the Diamond Light Source, beam line I04 using wavelength of 0.97949 Å with the Pilatus 6M-F detector system and processed at 1.75 Å resolution. The initial data processing of the form-I crystal proposed P32 symmetry. However data analysis after processing in P3 with XTRIAGE of the PHENIX package[30] observed clear

Table I
Crystallization and Crystal Handling

TbSLP	Crystallization conditions (well solution)[a]	Soaking solution[b]	Cryoprotectant solution[c]	Space group	Comments
Apo form-I	100 m*M* sodium citrate (pH 5.5), 10% (w/v) PEG4000, 200 m*M* sodium acetate		100 m*M* sodium citrate (pH 5.5), 25% (w/v) PEG4000, 200 m*M* sodium acetate	$P3_2$	PDB 5AB4
Apo form-II	100 m*M* sodium acetate (pH 4.6), 2.0*M* ammonium sulphate		100 m*M* sodium acetate (pH 4.6), 3.0*M* ammonium sulphate	$P3_2$	PDB 5AB5
CoA complex	100 m*M* sodium acetate (pH 4.6), 2.0 *M* ammonium sulphate	100 m*M* sodium acetate (pH 4.6), 2.2*M* ammonium sulphate, 10 m*M* CoA	100 m*M* sodium acetate (pH 4.6), 3.0*M* ammonium sulphate, 10 m*M* CoA	$P3_2$	No binding
Acetyl-CoA complex	100 m*M* sodium acetate (pH 4.6), 2.0*M* ammonium sulphate	100 m*M* sodium acetate (pH 4.6), 2.2*M* ammonium sulphate, 10 mM acetyl-CoA	100 m*M* sodium acetate (pH 4.6), 3.0*M* ammonium sulphate, 10 mM acetyl-CoA	$P3_2$	No binding
Acetoacetyl-CoA complex	100 m*M* sodium acetate (pH 4.6), 2.0*M* ammonium sulphate	100 m*M* sodium acetate (pH 4.6), 2.2*M* ammonium sulphate, 10 m*M* acetoacetyl-CoA	100 m*M* sodium acetate (pH 4.6), 3.0*M* ammonium sulphate, 10 mM acetoacetyl-CoA	$P2_1$	PDB 5AB6
Malonyl-CoA complex	100 m*M* sodium acetate (pH 4.6), 2.0*M* ammonium sulphate	100 m*M* sodium acetate (pH 4.6), 2.2*M* ammonium sulphate, 10 m*M* malonyl-CoA	100 m*M* sodium acetate (pH 4.6), 3.0*M* ammonium sulphate, 10 m*M* malonyl-CoA	$P2_1$	PDB 5AB7

[a]In all experiments the protein solution has been 5.0 mg/ml TbSLP in gel filtration buffer.
[b]Soaking at room temperature during 2 h.
[c]Short soak in cryobuffer, maximally for 30 sec.

twinning (using the H-test) (Table II). Data processing was continued in space group P3 using the XDS suite[31] and scaled using the AIMLESS program of the CCP4 suite.[32] Data from a form-II crystal was collected at Diamond Light Source, beam line IO3 and processed at 2.0 Å resolution. The XTRIAGE analysis suggested that the data set of the form-II crystal also had P3 (or $P3_1$, $P3_2$) symmetry with high twin fraction (Table II). The Matthews coefficient (V_m) calculation revealed that the P3 unit cell is compatible with two protein subunits in the asymmetric unit with V_m of 2.3 Å^3/Da and a solvent content of 47.3%. The structure was determined by the molecular replacement method. A polyalanine monomer model was constructed from the *L. mexicana* SCP2-thiolase structure (3ZBG)[16] using the program CHAINSAW of the CCP4 suite[32] and used as the initial search model in the calculations. The initial PHASER[33] run for the TbSLP structure determination suggested that the space group was $P3_2$. The PHASER Z-score for two monomers (chain A and B) placed in the asymmetric unit was 17.4. The PHASER model, along with the protein sequence was used as input for automated model building by the BUCCANEER[34] program of the CCP4 suite,[32] which resulted in a 78% complete model with $R_{work} = 26.9\%$ and $R_{free} = 34.9\%$. The model obtained from BUCCANEER was manually adjusted using the graphics program COOT[35] and refined with PHENIX.REFINE using the option for twin refinement. TLS refinement was not used. NCS restraints were applied using the default settings. The final model, refined at 1.75 Å resolution, has R_{work} and R_{free} of 19.9% and 21.5%, respectively (Table II). For the form-II crystal (Table I), refined at 2.0 Å resolution, the final refined structure has R_{work} and R_{free} of 19.8% and 22.0%, respectively (Table II).

For crystallographic ligand binding experiments, the crystals grown at the low pH were used (Table I), because all crystals grown at pH 5.5, stopped diffracting when transferred to a mother liquor containing malonyl-CoA or acetoacetyl-CoA. The concentration of these ligands was 10 m*M*. The crystal soaking protocol for malonyl-CoA and acetoacetyl-CoA did only work with some crystals grown in the drops of the low pH crystallization condition (Table I). The crystals were soaked for 2 h at room temperature and subsequently cryocooled. Further experimental details of the crystal handling steps are listed in Table I. The diffraction data of an acetoacetyl-CoA soaked crystal were collected at DLS beam line I04 and processed to 1.9 Å resolution whereas the diffraction data of the malonyl-CoA complexed crystal were collected at DLS beam line I03 and processed to 2.3 Å resolution. For these crystals the space group was found to be primitive monoclinic. XTRIAGE calculations with the datasets of these crystals did not detect twinning. All data were processed using the XDS suite[31] and scaled with the AIMLESS program of the CCP4 suite.[32] The Matthews coefficient (V_m) calculation (Table II) revealed that the unit cell of this primitive monoclinic crystal form is compatible with six protein subunits in the asymmetric unit. These structures were solved by PHASER using the monomer of the apo TbSLP coordinates as the phasing model. The calculations found six monomers (A, B, C, D, E, F) in the asymmetric unit with space group $P2_1$. The models were refined using REFMAC5[36]. Like in the refinement of the apo structures, NCS restraints were applied but TLS refinement

Table II
Data Collection and Refinement Statistics

	Typanosoma brucei SLP			
Data set[a]	Apo form-I	Apo form-II	Acetoacetyl-CoA complex	Malonyl-CoA complex
Unit cell data				
Space group	$P3_2$	$P3_2$	$P2_1$	$P2_1$
Cell parameters (Å, °)	*a*, *b* = 67.45, *c* = 157.1 α, β = 90, γ = 120	*a*, *b* = 66.69, *c* = 157.5 α, β = 90, γ = 120	*a* = 116.20, *b* = 65.97 *c* = 156.80 α, γ = 90, β = 90.03	*a* = 117.50, *b* = 66.40 *c* = 159.80 α, γ = 90, β = 91.18
V_m (Å^3/Dalton)	2.3	2.3	2.3	2.4
Number of subunits/asymmetric unit	2	2	6	6
Data collection				
Beam line	I04	I03	I04	I03
Wavelength (Å)	0.97949	0.97625	0.97949	0.97625
Temperature (K)	100	100	100	100
Resolution range (Å)	46.87–1.75 (1.78–1.75)	28.88–2.00 (2.05–2.00)	29.41–1.90 (1.93–1.90)	29.38–2.30 (2.34–2.30)
Total number of observed reflections	448,747 (24,572)	268,601 (19,755)	599,660 (29,362)	321,380 (14,166)
Number of unique reflections	80,250 (4388)	52,628 (3902)	184,266 (9142)	104,486 (5005)
R_{merge} (%)[b]	5.0 (136.5)	10.1 (125.1)	10.9 (75.4)	12.7 (71.9)
R_{pim} (%)[c]	2.3 (62.8)	5.0 (61.5)	7.1 (48.9)	8.3 (50.1)
CC1/2 (%)	99.8 (84.4)	99.7 (82.3)	99.5 (67.5)	98.2 (66.9)
Twinning operator (H-test)/fraction*	h,-h-k,-l/0.50	h,-h-k,-l/0.50	—	—
Mean $I/\sigma(I)$[d]	15.3 (1.0)	8.3 (1.3)	6.9 (2.2)	7.5 (1.9)
Completeness (%)	99.6 (98.1)	99.8 (99.0)	98.5 (98.5)	95.3 (93.7)
Multiplicity	5.6 (5.6)	5.1 (5.1)	3.3 (3.2)	3.1 (2.8)
Wilson B-factor (Å^2)	33.9	33.8	20.5	29.5
Refinement				
R_{work} (%)[e]	19.9	19.8	24.8	23.6
R_{free} (%)[f]	21.5	22.0	26.4	24.9
Number of reflections	79,395	52,602	174,242	98,670
No. of atoms	6085	6250	18,659	18,248
Protein atoms	5946	6066	17,634	17,560
Ligand atoms	—	—	324	324
Sulphate atoms	—	65	55	70
Solvent atoms	139	119	646	294
Model quality				
rmsD and rmsZ values[g]				
rms (bond length) (Å)	0.006	0.003	0.006	0.005
rmsZ (bond length)	0.34	0.24	0.33	0.30
rms (bond angle) (°)	1.2	0.9	1.1	1.0
rmsZ (bond angle)	0.57	0.46	0.54	0.52
Average B-factors (Å^2)				
Protein atoms	47.2	44.7	29.2	36.9
Ligand atoms of chains A/B/C/D/E/F			61.8/64.3/58.1/ 55.7/48.8/51.9	69.6/80.3/82.3/ 75.6/84.4/69.9
waters	41.7	37.6	33.1	32.1
Ramachandran plot (#)				
Most favored regions (%)	96.2	97.2	98.5	97.7
Allowed regions (%)	3.7	2.7	1.5	2.1
Outlier regions (%) (##)	0.1	0.1	0	0.2
PDB	5AB4	5AB5	5AB6	5AB7

[a]Values in parentheses refer to the highest resolution shell.
[b]R_{merge} = 100 * ($\Sigma_{hkl}\Sigma_i|I_i(hkl) - < I(hkl)>|)/\Sigma_{hkl}\Sigma_i < I_i(hkl)>$, where $I_i(hkl)$ is the intensity of the ith measurement of reflection (hkl) and $< I(hkl) >$ is its mean intensity.
[c]R_{pim} =100 * ($\Sigma_{hkl}[1/(N_{hkl}-1)]^{1/2}\Sigma_i|I_i(hkl) - < I(hkl) >|)/\Sigma_{hkl}\Sigma_i < I_i(hkl)>$, where $I_i(hkl)$ is the intensity of the ith measurement of reflection (hkl), $< I(hkl) >$ is its mean intensity and N is the number of measurements.
[d]*I* is the integrated intensity and $\sigma(I)$ is its estimated standard deviation.
[e]R_{work} = 100 * (Σ_{hkl}|Fo-Fcl)/Σ_{hkl}Fo where Fo and Fc are the observed and calculated structure factors.
[f]R_{free} is calculated as for R_{work} but from a randomly selected subset of the data (5%), which were excluded from the refinement calculations.
[g]The rms (bond length) and rms (bond angle) values were calculated by the refinement program and RMSZ values were calculated by the wwPDB validation server (for the protein parts).
(*) The twin operator was determined by XTRIAGE from PHENIX.[30] The twin fraction was determined in the refinement calculations.
(#) Calculated by Molprobity.[40]
(##) The residues in the outlier regions are part of high B-factor loops.

was not included. The final data collection and refinement statistics of these structures are listed in Table II.

The data of CoA and acetyl-CoA soaked crystals (grown at pH4.6, Table I) were collected at 2.2 Å resolution at the DLS beam line I04. In the structures of the acetyl-CoA and CoA soaked crystals no bound ligand was found in any of the active sites.

Structure analysis

The structural comparison of the apo TbSLP structure is described in detail with respect to the dimeric leishmanial SCP2-thiolase (3BZN, Lm-thiolase (C123A), complexed with CoA)[16] and the tetrameric *Z. ramigera* CT-thiolase (1DM3, acetylated thiolase complexed with acetyl-CoA, and 1M1O, the C89A variant complexed with acetoacetyl-CoA).[37,38] Both of these thiolases are short chain specific thiolases. With respect to the active site analysis comparisons have also been made with the human tetrameric T2-thiolase (2IBW)[11] for studying the possible mode of binding of the 2-methyl fatty acyl-CoA moiety and with the yeast dimeric AB-thiolase (1AFW)[12] for identifying the possible mode of binding of a long chain fatty acyl tail. All structural superpositions were performed using the SSM feature of COOT.[35,39] The geometry of the final models was examined using the programs Molprobity[40] and PROCHECK of the CCP4 suite.[32] Further structure analyses such as the B-factor profiles were analyzed using the program BAVERAGE of the CCP4 suite.[32] The PISA[41] webserver was used to identify dimer interface residues and evaluate dimeric interactions. All figures were made with PyMOL molecular-graphics software (v.1.2.1; Schrödinger). The Connolly surface of the dimeric TbSLP form-II structure was calculated with PyMOL using the surface cavity mode with a probe radius of 1.4 Å.

Bioinformatics

The human SCP2-thiolase domain sequence was used as the query sequence in a protein BLAST search against eight trypanosomatid genomes (*T. brucei, T. vivax, T. congolense, T. cruzi, L. mexicana, L. major, L. braziliensis, L. infantum*) available in the GeneDB (http://www.genedb.org/blast/submitblast/GeneDB_transcripts/omni), TriTrypDB (http://tritrypdb.org/tritrypdb/), and NCBI (http://blast.ncbi.nlm.nih.gov/Blast.cgi) databases to identify trypanosomatid SCP2-thiolase and SCP2-thiolase like proteins. Only sequences with the SCP2-thiolase fingerprints (CxS, HDCF, and GHP motifs) or SLP sequence fingerprints (YDCF) were included in the final set. The E-value cut off of 0.01 was used during all genome searches. One SCP2-thiolase and one SLP were identified in each of the eight trypanosomatid genomes. Subsequently, six mammalian genomes (human, *H. sapiens;* guinea pig, *C. porcellus*; pig, *S. scrofa*; cat, *F. catus;* chimpanzee, *P. troglodytes*; baboon, *P. anubis*) were searched with the sequences of human SCP2-thiolase and *T. brucei* SLP using the same criteria as in the trypanosomatid genome searches. One SCP2-thiolase was found in each of these genomes, but no SLP sequences were identified. Subsequently, a multiple sequence alignment of these eight parasite-specific SCP2-thiolases, and six mammalian SCP2-thiolases, together with the eight parasite-specific SLPs was prepared using ClustalW, as integrated in the program MEGA5.[42] The aligned sequences were used for construction of a phylogenetic tree using the neighbor-joining method with 10,000 bootstrap replicates in MEGA5.[42] A separate multiple sequence alignment was made using the two trypanosomatid SCP2-thiolases of known structure and the eight trypanosomatid SLPs to analyze the sequence conservation of these homologous protein sequences.

RESULTS

Bioinformatics studies

Bioinformatics studies were performed with the genomes of eight trypanosomatids, as listed in the Materials and Methods section. This analysis confirmed our earlier report[1] that a single SLP gene is present in the genome of each of these parasites, in addition to the SCP2-thiolase (type-2) gene. The alignment of the eight SLP amino acid sequences, together with those of the SCP2-thiolases (type-2) from *T. brucei* (Tb-thiolase) and *L. mexicana* (Lm-thiolase) shows the high sequence conservation of the SLPs (Supporting Information Fig. S1). This sequence analysis reveals that the SLPs possess the characteristic sequence fingerprint, YDCF in the Cβ2-Cα2 loop, which corresponds to HDCF in the SCP2-thiolases.

No SLP sequences were found in the six mammalian genomes analyzed (human, *H. sapiens;* guinea pig, *C. porcellus*; pig, *S. scrofa*; cat, *F. catus;* chimpanzee, *P. troglodytes*; baboon, *P. anubis*). Previous phylogenetic tree calculations[1] have shown that SLPs cluster as a separate class of thiolase sequences, being most closely related to the SCP2-thiolase type-1 (mammalian SCP2-thiolases) and type-2 (trypanosomal SCP2-thiolases), which are distantly related to the other thiolase sequence families. Indeed, sequences of the above listed eight SLPs, eight SCP2-thiolases (type-2), and six SCP2-thiolases (type-1) form three distinct groups in phylogenetic tree calculations (Supporting Information Fig. S2). The sequence identity between *T. brucei* SLP and the human SCP2-thiolase domain as calculated from a pairwise sequence alignment is 28.4%, whereas its identity with Lm-thiolase and Tb-thiolase is 20.0% and 20.5%, respectively. This human SCP2-thiolase (type-1) is involved in the bile acid synthesis pathway, where it catalyses the degradation

of bile acyl-CoA-intermediates that are characterized by a 2-methyl branched fatty acyl chain with a bulky steroid moiety at its ω-end. In contrast, the trypanosomal type-2 SCP2-thiolase has been found to have a small catalytic cavity and is predicted to be a functional biosynthetic thiolase of trypanosomal mitochondrial sterol biosynthesis,[16] although this remains to be experimentally confirmed.[43]

TbSLP is a mitochondrial protein

Antiserum raised against full-length TbSLP (Tb927.8.1820) expressed in *E. coli* failed to recognize the native protein in crude trypanosome extracts (data not shown). To determine its subcellular localization, recombinant TbSLP fused at the C-terminal (EGFP-TbSLP) or N-terminal (TbSLP-EGFP) extremity of the enhanced green fluorescent protein (EGFP) was inducibly expressed in EATRO1125. T7T procyclic cells, using the pLew100 vector. Fluorescence analyses of the TbSLP-EGFP cell line revealed a "mitochondrion-like" reticulate pattern of the recombinant TbSLP matching the mitochondrion-specific pattern observed in immunofluorescence assays with antisera directed against two *bona fide* trypanosomatid mitochondrial proteins, ASCT (acetate:succinate CoA-transferase),[44] and TDH (threonine dehydrogenase) (Fig. 3).[25] However, the EGFP-TbSLP recombinant protein showed a cytosolic-like pattern, suggesting that the N-terminal mitochondrial targeting motif is not functional when present in the middle of EGFP-TbSLP. One may thus consider that the N-terminal extremity of TbSLP contains a functional mitochondrial targeting sequence, consistent with the relatively high probability (0.63) predicted by Mitoprot (http://ihg.gsf.de/ihg/mitoprot.html).

TbSLP is involved in lipid metabolism in the procyclic form of *T. brucei*

To investigate the biological role of TbSLP in the procyclic form of *T. brucei*, the TbSLP gene was deleted by gene replacement as previously described.[26,45] Replacement of both TbSLP alleles by the puromycin and blasticidin selectable markers in the procyclic EATRO1125.T7T background was confirmed by PCR (Fig. 4). Both selected mutant cell lines (Δ*slp*-B6 and Δ*slp*-D3) showed growth retardation in both glucose-rich (20–29%) and glucose-depleted (38–53%) conditions, suggesting that TbSLP is important for growth, particularly in the insect midgut-like glucose-depleted environment (Fig. 4).

To investigate the impact of the TbSLP gene deletion on lipid metabolism, we determined the radiolabel incorporation from D-[U-^{14}C]-glucose and [1-^{14}C]-acetate into fatty acids and sterols in wild-type, Δ*slp*-B6 and Δ*slp*-D3 procyclic cells, incubated for 16 h in SDM79 medium. Fatty acid methyl esters (FAMEs) from total lipids were formed by transesterification, separated from sterols by High Performance Thin Layer Chromatography (HPTLC), and the radiolabeling of FAMEs and sterols was then determined (Fig. 5). The amounts of label from both acetate and glucose incorporated into fatty acids and sterols is respectively ∼2-fold and ∼5.3-fold reduced in both Δ*slp* mutants compared to wild-type cells, suggesting that TbSLP is directly or indirectly involved in lipid biosynthesis.

Solution properties of TbSLP

The TbSLP construct, with a $(His)_6$-tag at its N-terminus, was expressed in *E. coli* BL21(DE3) containing also the pGro7 plasmid encoding the chaperones GroEL and GroES. TbSLP was purified using three chromatography steps, involving a His-tag affinity column, an anion exchange column, and a gel filtration column. Gel filtration experiments followed up by SLS measurements showed that TbSLP elutes as a dimer, with a molecular mass of 88 kDa (Supporting Information Fig. S3). In order to study the enzymological properties of TbSLP, several assays with CoA, acetyl-CoA, acetoacetyl-CoA and malonyl-CoA were carried out, taking into account that TbSLP could be a thiolase, a malonyl-CoA decarboxylase[46] or a malonyl-CoA:ACP-transacylase.[47] The spectrophotometric thiolase assays of TbSLP (under the conditions as described in the Materials and Methods section) revealed only residual activity in the degradative direction (using acetoacetyl-CoA as the substrate), being 0.02 μmole/min/mg, whereas in the synthetic direction (using acetyl-CoA as the substrate), no formation of acetoacetyl-CoA could be detected. The degradative conversion was confirmed by mass spectrometry experiments, which showed that incubation of TbSLP with acetoacetyl-CoA and CoA resulted in the formation of acetyl-CoA (Supporting Information Fig. S4).

High Performance Liquid Chromatography (HPLC) approaches were also used to study the possible catalytic properties of TbSLP. No thioesterase activity could be detected when the enzyme was incubated with acetyl-CoA, acetoacetyl-CoA or malonyl-CoA alone. The possible thiolytic cleavage of acetoacetyl-CoA could not be measured by HPLC because acetoacetyl-CoA (the substrate) and acetyl-CoA (the product) elute at exactly the same position in the chosen experimental setup. In the case of incubation with malonyl-CoA, a residual decarboxylase activity was observed with an estimated k_{cat} of 0.005 sec^{-1} and apparent K_m of 31 μM (Fig. 6). Product analysis by mass spectrometry of malonyl-CoA incubation mixtures showed that TbSLP slowly decarboxylates malonyl-CoA into acetyl-CoA (confirming also that the HPLC product is acetyl-CoA) (Fig. 7).

SPR ligand binding assays were done to analyze the affinity of different fatty acyl-CoA derivatives (acetyl-CoA, acetoacetyl-CoA and malonyl-CoA), including also

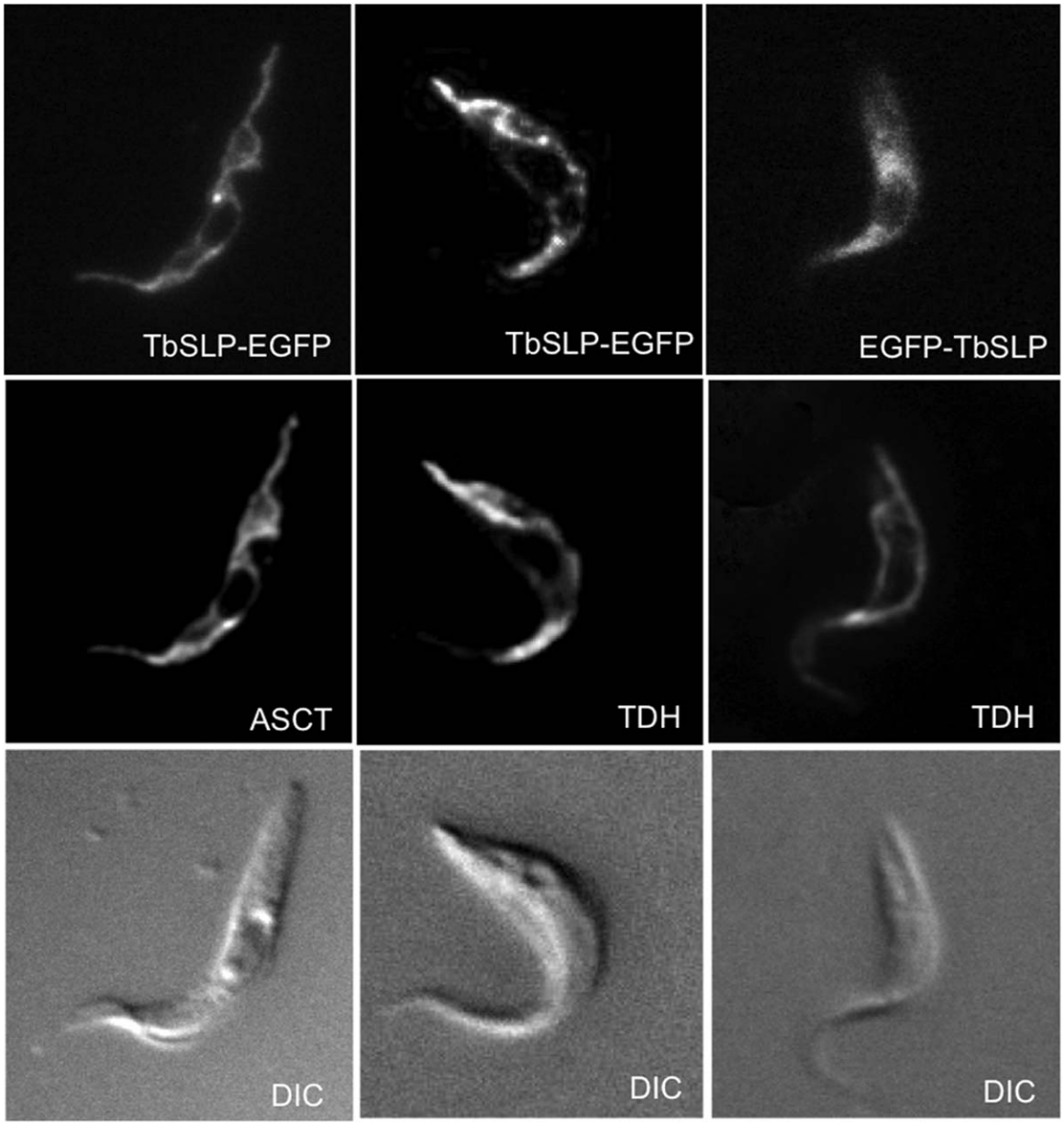

Figure 3

Mitochondrial localization of TbSLP. The top panel shows fluorescent procyclic trypanosomes expressing TbSLP-EGFP and EGFP-TbSLP, which refer to recombinant Enhanced Green Fluorescent Protein (EGFP) fused at the C-terminal and N-terminal extremity of TbSLP, respectively. TbSLP-EGFP expressing cells were stained with rabbit anti-ASCT and anti-TDH antisera, which specifically recognized mitochondrial proteins.[25,44] EGFP-TbSLP expressing cells were stained with rabbit anti-TDH antiserum. Cells were incubated with Alexa Fluor 594 anti-rabbit IgG conjugate before analyses by immunofluorescence (central panel). The bottom panel shows Differential Interference Contrast (DIC) imaging of the same cells.

CoA. The affinity of TbSLP for CoA and acetyl-CoA was very low, precluding the measurement of K_d values, whereas for acetoacetyl-CoA a K_d of 0.9 m*M* was found (Supporting Information Fig. S5). With the SPR binding assay a high affinity for malonyl-CoA was measured, the K_d being approximately 90 μM (Supporting Information Fig. S5), in agreement with the HPLC data.

Structure description and mode of binding of acyl-CoA

The crystal structure of TbSLP was determined by molecular replacement using the structure of a monomer of the *L. mexicana* C123A SCP2-thiolase (Lm-thiolase; 3ZBN)[16] as the initial phasing model (this model has 20% sequence identity with TbSLP) (Fig. 2). The two

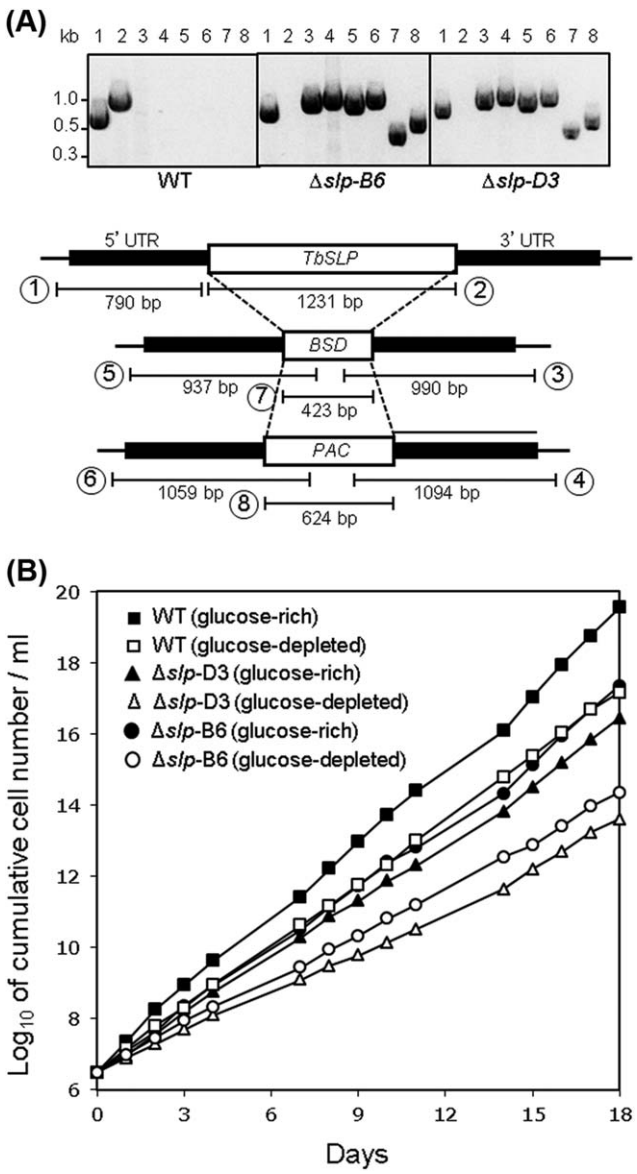

Figure 4

Construction of the Δ*slp T. brucei* procyclic cell lines. **A.** PCR analysis of genomic DNA isolated from the parental wild-type and the mutant Δ*slp*-B6 and Δ*slp*-D3 cell lines. The PCR amplifications were performed with primers based on sequences that flank the 5'UTR (5'UTRct primer) and 3'UTR (3'UTRct primer) fragments used to target the TbSLP gene depletion (black boxes). The PCR-products are labeled from 1 to 8. The primers used to PCR amplify product 1 are the 5'UTRct primer and a primer corresponding to the 3'-extremity of the 5'UTR. For PCR products 3–6 internal primers of the blasticidin (*BSD*, PCR products 5 and 3) and puromycin (*PAC*, PCR products 6 and 4) resistance genes were used in combination with the 5'UTRct or 3'UTRct primers. The TbSLP, *BSD* and *PAC* coding sequences were also PCR-amplified with specific primers (PCR products 2, 7 and 8, respectively). As expected, PCR amplification of the TbSLP gene was only observed in wild-type cells, while *BSD* and *PAC* PCR-products were observed only in the Δ*slp* cell lines. **B.** Growth curves of the wild-type (WT), Δ*slp*-B6 and Δ*slp*-D3 cell lines, grown in glucose-rich and glucose-depleted conditions.

apo structures and the two ligated structures have been refined at resolutions ranging from 1.75 Å (apo, form-I) and 2.00 Å (apo, form-II) to 1.90 Å (acetoacetyl-CoA) and 2.30 Å (malonyl-CoA). There are no significant differences between the structures of form-I (grown in the presence of 10% PEG 4000, pH = 5.5) and form-II (grown in the presence of 2.0 M ammonium sulphate, pH = 4.6). In each of the subunits there are three flexible loops, regions 70–81, 223–243, and 258–268, which have high B-factors and some of these regions have not been built completely, in particular the 223–243 region. These three loops are located in regions far away from the active site.

Chain B of the TbSLP form-I has been used for the comparative structural studies. This structure has been refined to R_{work} (19.9%) and R_{free} (21.5%) (Table II). The crystallographic binding studies have been done with crystals grown at the low pH crystallization condition. In these crystal structures the mode of binding of acetoacetyl-CoA and malonyl-CoA in the respective binding pockets is clearly defined in the electron density maps. In the soaking experiments with CoA and acetyl-CoA no binding was observed, in agreement with the low affinity of TbSLP for these compounds. Chain E of the acetoacetyl-CoA complex and chain D of the malonyl-CoA complex were used in the structure analysis unless otherwise stated. In these subunits the acetoacetyl- and malonyl- moieties are also well defined by the respective electron density maps (Supporting Information Fig. S6). The mode of binding of acetoacetyl-CoA and malonyl-CoA to SLP is shown in Figure 8.

The secondary structure assignment of TbSLP is provided in Figure 2. The two subunits of TbSLP form a tight dimer (Fig. 9). The structure analysis using the PISA server suggests that the physiological oligomeric state of TbSLP is a dimer in agreement with the SLS data and the mode of dimerization is mediated by Nβ3 (Fig. 9), running antiparallel to the Nβ3 of the second subunit like for canonical thiolases. Comparison of the TbSLP structure with Lm-thiolase shows that the loop after Nβ1 is much shorter, whereas the loop after Cα2 is much more extended (Figs. 2 and 10). The Cβ1-Cα1 loop is also longer. Major structural differences are also seen in the TbSLP loop domain (Fig. 10). The structural superposition of the loop domain of the *Z. ramigera* CT-thiolase, the leishmanial SCP2-thiolase (type-2) and TbSLP shows that the tetramerization loop and the cationic loop of the *Z. ramigera* CT-thiolase are missing in TbSLP (as well as in Lm-thiolase) (Fig. 10). The Lα1 helix, covering the active site, is much more extended in the TbSLP structure. The structural differences in the loop domain of TbSLP result in a different mode of binding of the adenine moieties of CoA, whereas the pantetheine moieties superimpose well (Fig. 10). In TbSLP the adenine ring is stacked between the side chains of Leu205 and Arg210. Only few hydrogen bond

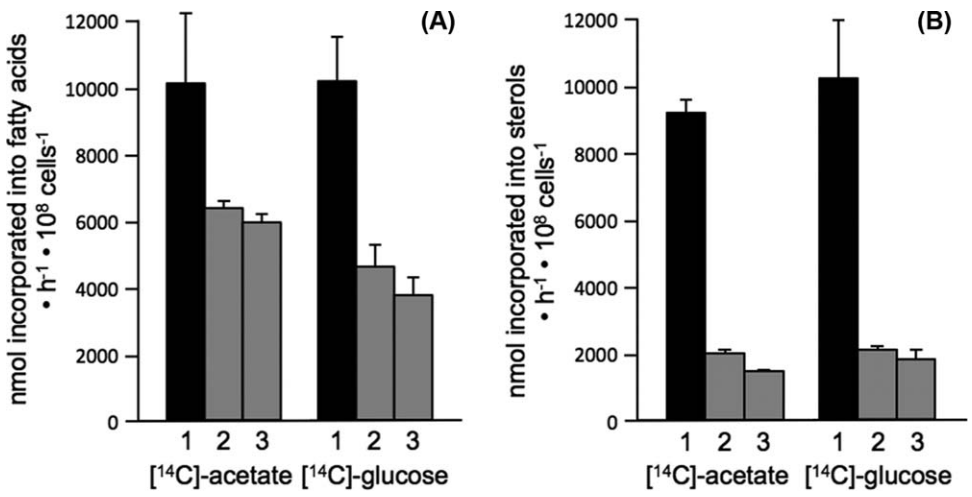

Figure 5

Incorporation of radiolabel from [1-^{14}C]-acetate and D-[U-^{14}C]-glucose into lipids of procyclic trypanosomes. **A.** Incorporation in fatty acids. **B.** Incorporation in sterols. ^{14}C-labeled fatty acid methyl esters and sterols were separated by HPTLC after transesterification and analyzed as described in the Materials and Methods section. Wild-type (EATRO1125.T7T, lane 1), Δ*slp*-B6 (lane 2), and Δ*slp*-D3 (lane 3) procyclic cells were incubated for 16 h in SDM79 containing 4 m*M* glucose with D-[U-^{14}C]-glucose or with 1 m*M* acetate and [1-^{14}C]-acetate, prior to lipid extraction. The data are expressed as nmole of acetate or glucose (radioactive and non-radioactive molecules) incorporated into fatty acids (**A**) or sterols (**B**) in 10^8 cells per hour. Error bars indicate mean ± standard deviation of three independent experiments.

interactions between the CoA moiety and the protein are present (Fig. 10). The N6A atom of the adenine moiety is hydrogen bonded with the main chain oxygens of Leu205 and Cys208 of the pantetheine loop. Salt bridges are present between NH2(Arg197) and NH2(Arg211) and the pyrophosphate moiety, which is also hydrogen bonded to OG(Ser122) of helix Lα1. There are no strong hydrogen bonds (less than 3.5 Å) with the pantetheine moiety (Fig. 10). Instead, it is surrounded by hydrophobic residues including Phe125, Ile143, Pro144, Ala209, Cys299, Phe300, Trp357 as well as two waters, which are shown in Figure 10.

Catalytic site of TbSLP

The putative active site of TbSLP is deeply buried in the core, below Lα1 (residues 123–133) and Lα2 (residues, 142–157) of the loop domain. The side chains and main chain segments which outline the active site are well defined in the electron density maps of each of the four structures and there are no structural changes between the apo enzyme and the ligated complexes.

Also in the active sites the ligand binding does not induce structural changes, like also observed for ligand binding in the thiolase active site.[37,38] The YDCF-loop of Lm-thiolase and TbSLP adopts the same conformation (Fig. 11). The binding mode of the acetoacetyl- and malonyl-moieties to TbSLP is the same (Fig. 12), but the affinity of TbSLP for malonyl-CoA is much higher than for acetoacetyl-CoA. The 3-keto oxygen of acetoacetyl-CoA and the corresponding oxygen of malonyl-CoA bind in OAH2 (Fig. 12). This 3-keto oxygen replaces a water molecule that is bound at this site in the apo structures. The terminal carbon and corresponding carboxylate oxygen atom of the acetoacetyl- and malonyl-moieties, respectively, point to the Trp357 side-chain (Figs. 8 and 12). This tryptophan is conserved in the SLPs (Supporting Information Fig. S1). The non-planar conformation is probably unfavorable for the acetoacetyl moiety, which correlates with its low affinity. The high affinity for the

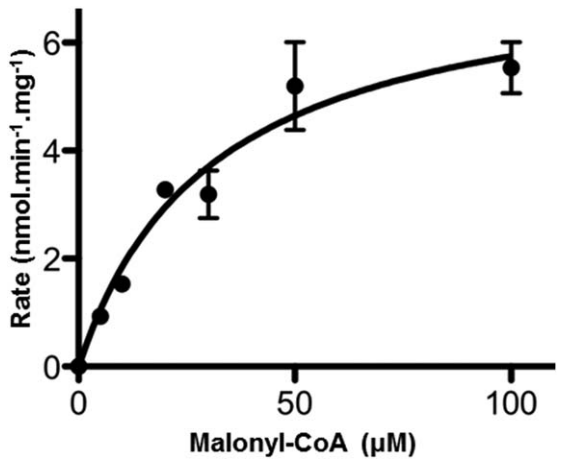

Figure 6

Kinetics of malonyl-CoA decarboxylation as measured by HPLC. TbSLP was incubated at room temperature, for 30 min, in the presence of different concentrations of malonyl-CoA and the formation of acetyl-CoA was quantified by HPLC.

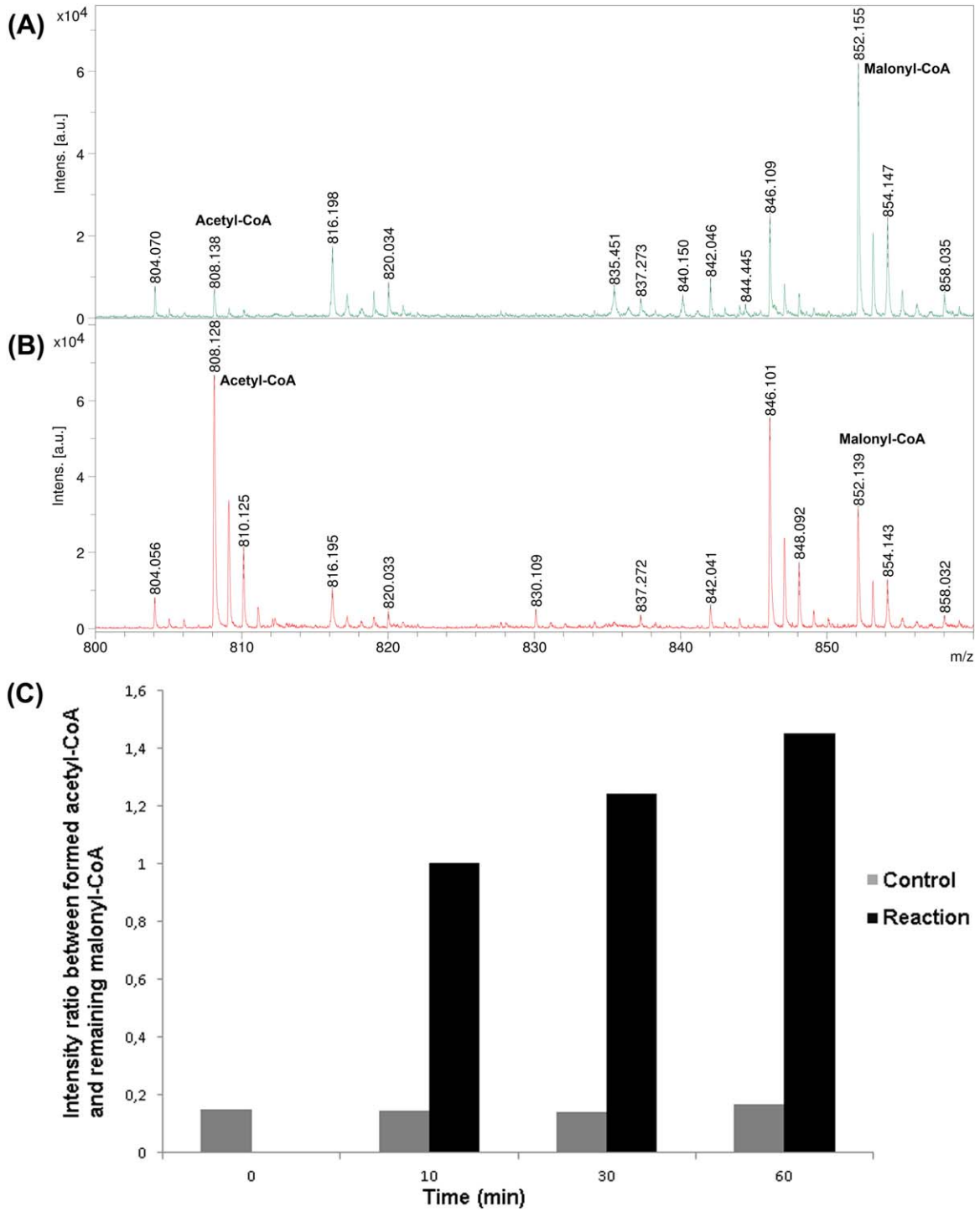

Figure 7

Mass spectrometry experiments concerning the decarboxylase activity of TbSLP. All reaction incubations were done at room temperature. **A.** The mass spectrum of the control reaction mixture, incubated for 2 h without addition of TbSLP. **B.** The mass spectrum of the reaction mixture containing 50 μM malonyl-CoA and 10 μg TbSLP and incubated for 2 h, shows that malonyl-CoA is slowly converted to acetyl-CoA. **C.** The ratio of the acetyl-CoA/malonyl-CoA peak heights of the mass spectra increases as a function of time. The values are averages of three measurements. [Color figure can be viewed in the online issue, which is available at wileyonlinelibrary.com.]

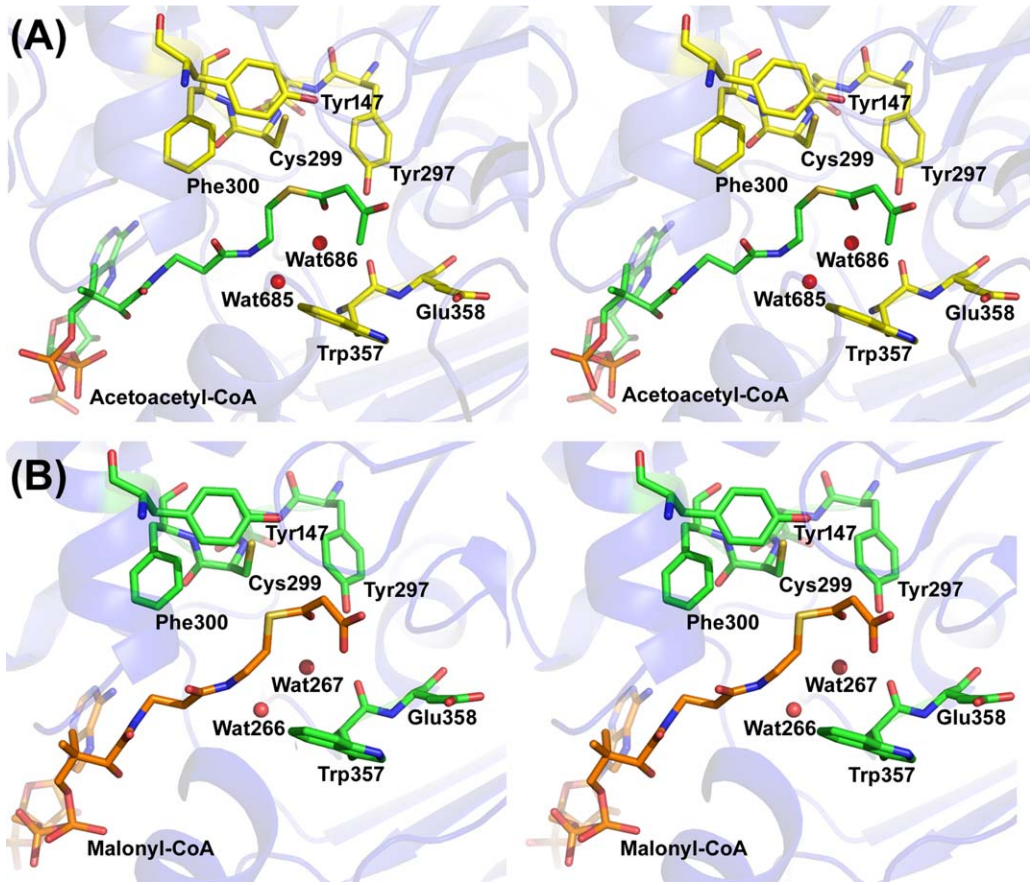

Figure 8

Structure of TbSLP complexed with acetoacetyl-CoA and malonyl-CoA. **A.** Stereo figure of the TbSLP chain E active site with the ligand acetoacetyl-CoA (green). The YDCF (Cβ2-Cα2) loop and the WE (Cβ3-Cα3) motif are highlighted as yellow stick models. **B.** Stereo figure of the TbSLP chain D active site with bound malonyl-CoA (orange). The YDCF (Cβ2-Cα2) loop and the WE (Cβ3-Cα3) motif are highlighted as green stick models. Two water molecules near OAH1 are shown as red spheres.

malonyl-CoA correlates with the tight hydrogen bond interactions of the negatively charged oxygen of its carboxylate moiety with the OAH2 hydrogen bond donors (Fig. 12).

TbSLP does not have any of the five conserved thiolase sequence fingerprints suggesting that TbSLP is not a *bona fide* thiolase enzyme. The nucleophilic cysteine of the CxS motif (Cys89 in the *Z. ramigera* CT-thiolase, which (in the degradative direction) reacts with the 3-keto carbon of the fatty acyl-CoA, is replaced by Gly87 in TbSLP (Fig. 2). The NEAF of the Cβ2-Cα2 motif is replaced by YDCF. The histidine of the GHP loop, which deprotonates the nucleophilic cysteine, is replaced by the alanine of the GAP loop of TbSLP, and the CxG motif of the Cβ4-Cβ5 loop is replaced by NGG in the TbSLP structure (Figs. 1 and 2). The Asn393 of the latter motif points into the TbSLP active site. In SCP2-thiolase the corresponding residue is a methionine (Met426). In SCP2-thiolase, the function of the canonical CxG cysteine (which is the acid/base) is replaced by the cysteine of the HDCF loop.[16] In TbSLP the sequence of this loop is YDCF. The TbSLP cysteine and the SCP2-thiolase cysteine side chains superpose precisely (Fig. 11). The two thiolase OAHs are also present in TbSLP. OAH1 (for binding the thioester oxygen of acetoacetyl-CoA and malonyl-CoA) is formed by OH(Tyr297) and W686. W686 forms a dyad with another active site water (W685) (Fig. 10). OAH2 (for binding the 3-keto oxygen of acetoacetyl-CoA and one of the carboxylate oxygens of malonyl-CoA) is formed by NH(Gly87) and NH(Gly395) (Fig. 12). The active site residues pointing toward the acetoacetyl/malonyl moiety are Tyr297 and Cys299 of the YDCF-loop, Tyr147 of Lα2, and Trp357 (of the Cβ3-Cα3 loop) (Figs. 11 and 12). These active site residues are fully conserved in other SLP sequences (Supporting Information Fig. S1). The side-chain of the conserved Cys299 is hydrogen bonded to Tyr147, Cys303, Asn393 as well as N(Cys299) and N(Phe300). Only the latter hydrogen bonds, which are with the main chain N-atoms, are also present in the structures of the SCP2-

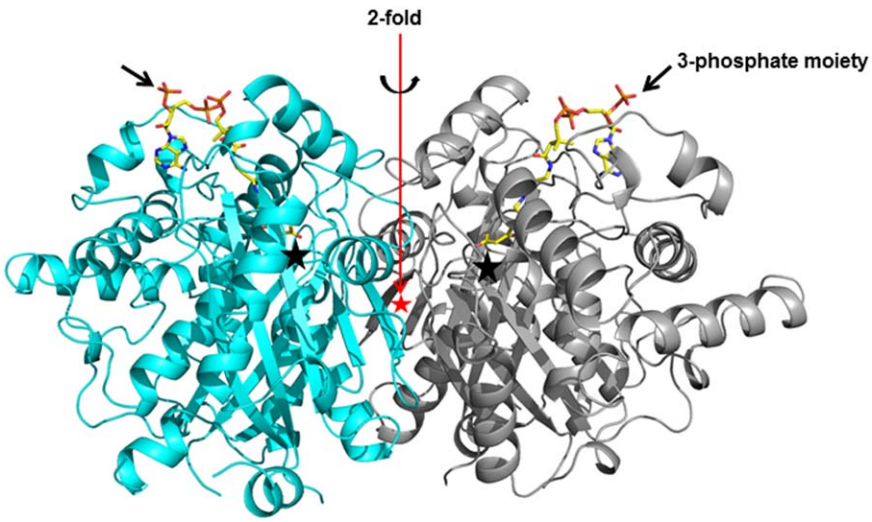

Figure 9

Dimeric structure of SCP2-thiolase like protein (SLP) of *T. brucei* in complex with acetoacetyl-CoA. Chain A and B are colored cyan and grey, respectively. The mode of dimerization is mediated by Nβ3 (labeled by a red *). The catalytic sites (labeled by a black *) are deeply buried. The 3-phosphate moieties (indicated by arrows) of acetoacetyl-CoA are solvent exposed.

thiolases. The hydrogen bond interactions of the YDCF-cysteine (Cys299) present in TbSLP (with Tyr147, Cys303 and Asn393) would stabilise the deprotonated cysteine. These hydrogen bond interactions are not present in the SCP2-thiolases, as Tyr147 corresponds to Phe186, Cys303 to Ala344 and Asn393 to Met426 (Fig. 11, Supporting Information Fig. S1).

DISCUSSION

Bioinformatics studies identified SLP as an SCP2-thiolase like protein.[1] Interestingly, in these calculations it was also found that there are two types of SCP2-thiolases, being referred to as type-1 and type-2. Is SLP a type-1 or type-2 like enzyme? The phylogenetic calculations did not provide an unambiguous answer on this question (see also Supporting Information Fig. S2). The type-1 SCP2-thiolase functions in the bile acid synthesis pathway and its substrate is therefore a 2-methyl branched fatty acid molecule with a bulky steroid moiety at its ω-end.[48] The crystal structure of the type-1 SCP2-thiolase is not yet known. It is expected to have a rather open active site, such that it can bind the bulky steroid moiety. However, the SCP2-thiolase (type-2) crystal structure is known; its active site is rather tight and deeply buried, just being able to bind acetoacetyl-CoA.[16] Enzyme kinetic studies have indeed shown that this type-2 SCP2-thiolase is a biosynthetic thiolase that can efficiently catalyze the formation of acetoacetyl-CoA from two molecules of acetyl-CoA. Interestingly, the crystal structure of TbSLP demonstrates that its active site is also deeply buried and very tight, like in the type-2 SCP2-thiolase. Further structural comparisons have been done with the T2-thiolase (which can degrade 2-methyl-acetoacetate-CoA),[11] the *Z. ramigera* CT-thiolase[37] and long-chain, unbranched, degradative yeast AB-thiolase.[12] From the structural studies of the T2-thiolase it is known that its Cβ1-Cα1 loop provides space for binding the 2-methyl group of its substrate.[11] In *Z. ramigera* CT-thiolase and in the long-chain degradative AB-thiolase this loop has the VMG-motif (Fig. 2), and in these structures there is no space for the 2-methyl group. The structural comparisons of TbSLP with the T2-thiolase (2IBW),[11] the *Z. ramigera* thiolase (1DM3),[37] and the AB-thiolase (1AFW)[12] suggest that the TbSLP binding pocket does also not allow binding of a 2-methyl moiety. In this respect the TbSLP active site pocket is therefore similar to that of the leishmanial SCP2-thiolase (type-2).[16] A cavity analysis of the apo structure (form-II) by PyMOL also suggests that the active site does not have any additional space to accommodate fatty acyl tails that are more extended than the acetoacetyl/malonyl moiety (Supporting Information Fig. S7).

The active site has high affinity for malonyl-CoA (Fig. 6), suggesting that this acyl-CoA form could be a substrate of TbSLP. The malonyl moiety of malonyl-CoA is bound in a twisted conformation such that the carboxylate moiety is positioned perpendicular to the thioester moiety. This perpendicular arrangement causes the carboxylate to be an easy leaving group.[49] The YDCF-cysteine could protonate the remaining acetyl moiety such that the products are acetyl-CoA and CO_2. Nevertheless, the decarboxylase activity is rather low,

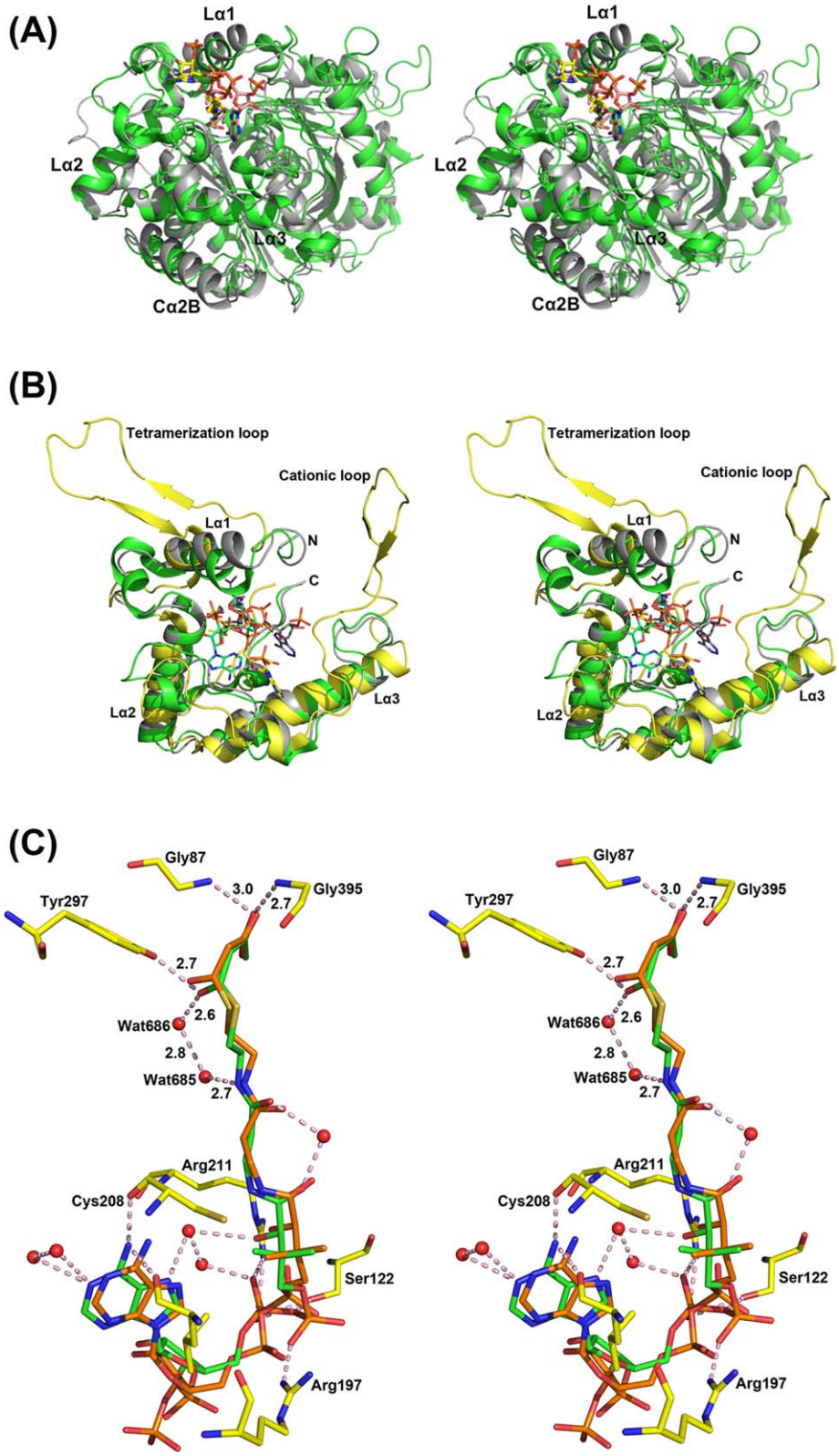

Figure 10

The structure description of TbSLP. **A.** The superposition of the overall fold of the TbSLP complex with acetoacetyl-CoA chain E (grey) on the *L. mexicana* SCP2-thiolase (Lm-thiolase) complex with CoA chain B (3ZBN) (green). The ligands acetoacetyl-CoA (light purple) and CoA (yellow) are shown as stick models. **B.** The superposition of the loop domain of the TbSLP complex with acetoacetyl-CoA chain E (grey), the Lm-thiolase complex with CoA chain B (3ZBN) (green) and the *Z. ramigera* CT-thiolase complex with acetyl-CoA chain B (1DM3) (yellow). The tetramerization loop and cationic loop of *Z. ramigera* CT-thiolase are absent in TbSLP and in Lm-thiolase, whereas the Lα1 helix of TbSLP is much more extended in comparison to the Lm-thiolase and *Z. ramigera* CT-thiolase. N and C label the N-terminus and C-terminus of the loop domain, respectively. **C.** Superposition of acetoacetyl-CoA (green) and malonyl-CoA (orange), as bound to SLP, shows that the conformations of the bound ligands are similar. The hydrogen bond interactions shorter than 3.5 Å between acetoacetyl-CoA and TbSLP and water molecules are highlighted by dotted lines.

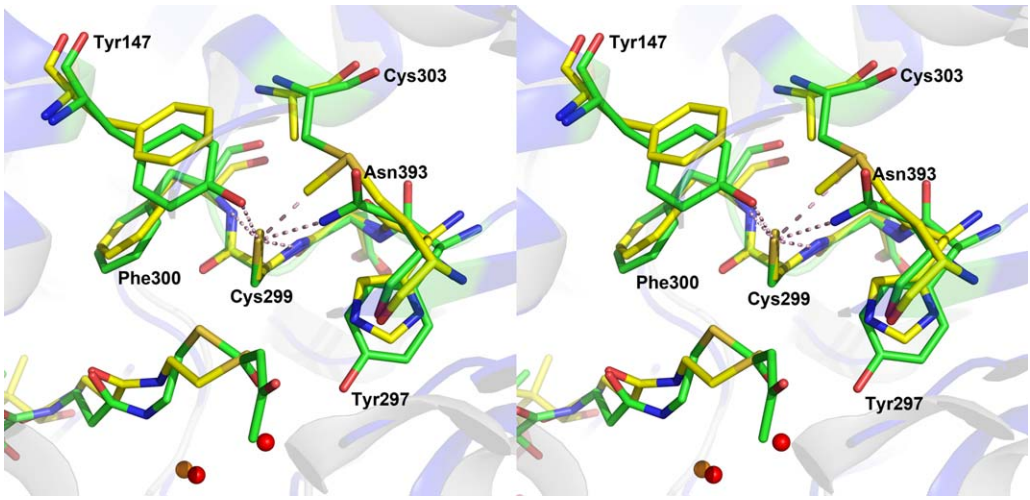

Figure 11

The active site superposition of TbSLP (green) and Lm-thiolase (3ZBN) (yellow) shows that the HDCF-loop of Lm-thiolase superposes well on the YDCF-loop of TbSLP. The SG(Cys299) of the YDCF-loop of TbSLP interacts with five hydrogen bond donors: OH(Tyr147), NH(Cys299), NH(Phe300), SG(Cys303), and ND2(Asn393).

suggesting that this is not the real function. Indeed, the *T. brucei* genome encodes for an annotated malonyl-CoA decarboxylase (Tb927.8.1060), which is predicted to contain a mitochondrial target signal with a high confidence score (0.69) using the MITOPROT program and has been detected in the *T. brucei* mitochondrial proteome.[50] Alternatively, TbSLP may be active as a malonyl-CoA transacylase. The YDCF-cysteine could act as a nucleophile, in which case the competent state is the thiolate form of the deprotonated cysteine. The hydrogen bond environment of the YDCF-cysteine would stabilise this negative charge, as discussed in the preceding section (Fig. 11). In any case, at the low pH of the soaking buffer of the crystalline TbSLP the reactive YDCF-cysteine will be protonated which then suggests that in these crystals the YDCF-cysteine is not activated for nucleophilic attack. Interestingly, no conversion of acetoacetyl-CoA and malonyl-CoA is detected when the

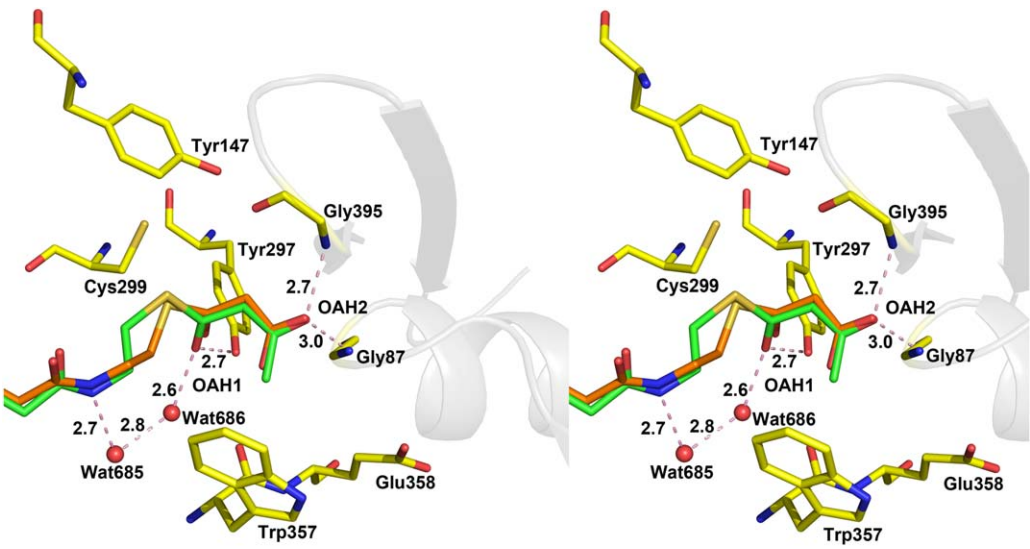

Figure 12

The oxyanion holes OAH1 and OAH2 of the thiolase fold are preserved in TbSLP. OAH1 is formed by OH(Tyr297) and Wat686 (forming a dyad with Wat685) whereas OAH2 is formed by NH(Gly87) and NH(Gly395). The acetoacetyl-CoA is colored green and the malonyl-CoA is colored orange.

crystal is soaked with these substrates at pH 4.6, whereas at pH 5.5 the crystals deteriorate when soaked with acetoacetyl-CoA or malonyl-CoA. If the YDCF cysteine acts as a nucleophile, then the function of the enzyme could be a malonyl-CoA transacylase, such as a malonyl-CoA:ACP transacylase (MCAT), transferring the malonyl moiety from CoA to ACP via a covalent malonylated intermediate.[47,51–55] Malonyl-ACP is a substrate in fatty acid synthesis reactions. In well characterized MCATs of the fatty acid synthesis FAS I and FAS II pathways the nucleophile is a serine[47] and an OAH is proposed also to be important in the reaction mechanism. Reported apparent affinity constants (K_mś measured in the presence of ACP) are in the range of 5 μM to 20 μM.[47,56,57] The mitochondrial MCAT apparently has low affinity for acetyl-CoA.[47,53] Other malonyl-CoA transacylases have also been described.[58]

The two well preserved OAHs (Fig. 12) and the tight binding of malonyl-CoA suggest that TbSLP is an enzyme functioning in malonyl-CoA metabolism. The decreased production of fatty acids from glucose and acetate in the knockout Δ*slp* procyclic cells is consistent with the notion that TbSLP could be a malonyl-CoA:ACP transacylase, since malonyl-ACP is the elongator of fatty acid synthesis in the trypanosomal mitochondrial FAS-II system.[59] In contrast, the endoplasmic reticulum elongase system uses malonyl-CoA as elongator and should not be affected by the SLP gene deletion.[60] Decrease of sterol biosynthesis could be a secondary effect linked to reduction of fatty acid biosynthesis as we recently observed for other mutants affected in fatty acid production from glucose, threonine or acetate (our unpublished data). Interestingly, the decreased growth rates of Δ*slp* mutants in glucose-rich and glucose-depleted conditions suggest that the TbSLP function is important for optimal growth whatever the carbon source used to feed the central metabolism of the procyclic trypanosomes. So far, the SLP gene has only been observed in trypanosomatid genomes, with no evidence for its presence in mammalian genomes, suggesting that the enzyme is involved in a unique pathway not present in the mammalian host.

ACKNOWLEDGMENTS

The use of the facilities and expertise of the Biocenter Oulu crystallization, data collection, and proteomics core facility, a member of Biocenter Finland and Instruct-FI, is gratefully acknowledged. The intensity data sets used for the refined structures were collected at Diamond and the support from the Diamond staff of beam lines I03 and I04 is gratefully acknowledged. We thank Dr. Barycki (University of Nebraska) for providing the plasmid of the human L-3-hydroxyacyl-CoA dehydrogenase. We thank the reviewers for insightful comments on the description of the used protein crystallographic protocols.

REFERENCES

1. Anbazhagan P, Harijan RK, Kiema TR, Janardan N, Murthy MR, Michels PA, Juffer AH, Wierenga RK. Phylogenetic relationships and classification of thiolases and thiolase-like proteins of *Mycobacterium tuberculosis* and *Mycobacterium smegmatis*. Tuberculosis (Edinb) 2014;94:405–412.
2. Janardan N, Harijan RK, Wierenga RK, Murthy MR. Crystal structure of a monomeric thiolase-like protein type 1 (TLP1) from *Mycobacterium smegmatis*. PLoS One 2012;7:e41894
3. Haapalainen AM, Merilainen G, Wierenga RK. The thiolase superfamily: condensing enzymes with diverse reaction specificities. Trends Biochem Sci 2006;31:64–71.
4. Cronan JE. The chain-flipping mechanism of ACP (acyl carrier protein)-dependent enzymes appears universal. Biochem J 2014;460: 157–163.
5. Whicher JR, Dutta S, Hansen DA, Hale WA, Chemler JA, Dosey AM, Narayan AR, Hakansson K, Sherman DH, Smith JL, Skiniotis G. Structural rearrangements of a polyketide synthase module during its catalytic cycle. Nature 2014;510:560–564.
6. Shafqat N, Turnbull A, Zschocke J, Oppermann U, Yue WW. Crystal structures of human HMG-CoA synthase isoforms provide insights into inherited ketogenesis disorders and inhibitor design. J Mol Biol 2010;398:497–506.
7. Miziorko HM. Enzymes of the mevalonate pathway of isoprenoid biosynthesis. Arch Biochem Biophys 2011;505:131–143.
8. Jiang C, Kim SY, Suh DY. Divergent evolution of the thiolase superfamily and chalcone synthase family. Mol Phylogenet Evol 2008;49: 691–701.
9. Kursula P, Sikkila H, Fukao T, Kondo N, Wierenga RK. High resolution crystal structures of human cytosolic thiolase (CT): a comparison of the active sites of human CT, bacterial thiolase, and bacterial KAS I. J Mol Biol 2005;347:189–201.
10. Kiema TR, Harijan RK, Strozyk M, Fukao T, Alexson SE, Wierenga RK. The crystal structure of human mitochondrial 3-ketoacyl-CoA thiolase (T1): insight into the reaction mechanism of its thiolase and thioesterase activities. Acta Crystallogr D Biol Crystallogr 2014; 70:3212–3225.
11. Haapalainen AM, Merilainen G, Pirila PL, Kondo N, Fukao T, Wierenga RK. Crystallographic and kinetic studies of human mitochondrial acetoacetyl-CoA thiolase: the importance of potassium and chloride ions for its structure and function. Biochemistry 2007; 46:4305–4321.
12. Mathieu M, Modis Y, Zeelen JP, Engel CK, Abagyan RA, Ahlberg A, Rasmussen B, Lamzin VS, Kunau WH, Wierenga RK. The 1.8 A crystal structure of the dimeric peroxisomal 3-ketoacyl-CoA thiolase of *Saccharomyces cerevisiae*: implications for substrate binding and reaction mechanism. J Mol Biol 1997;273:714–728.
13. Oeljeklaus S, Fischer K, Gerhardt B. Glyoxysomal acetoacetyl-CoA thiolase and 3-oxoacyl-CoA thiolase from sunflower cotyledons. Planta 2002;214:597–607.
14. Venkatesan R, Wierenga RK. Structure of mycobacterial beta-oxidation trifunctional enzyme reveals its altered assembly and putative substrate channeling pathway. ACS Chem Biol 2013;8: 1063–1073.
15. Ishikawa M, Tsuchiya D, Oyama T, Tsunaka Y, Morikawa K. Structural basis for channelling mechanism of a fatty acid beta-oxidation multienzyme complex. Embo J 2004;23:2745–2754.
16. Harijan RK, Kiema TR, Karjalainen MP, Janardan N, Murthy MR, Weiss MS, Michels PA, Wierenga RK. Crystal structures of SCP2-thiolases of Trypanosomatidae, human pathogens causing widespread tropical diseases: the importance for catalysis of the cysteine of the unique HDCF loop. Biochem J 2013;455:119–130.

17. Merilainen G, Poikela V, Kursula P, Wierenga RK. The thiolase reaction mechanism: the importance of Asn316 and His348 for stabilizing the enolate intermediate of the Claisen condensation. Biochemistry 2009;48:11011–11025.
18. World Health OrganizationResearch priorities for Chagas disease, human African trypanosomiasis and leishmaniasis. World Health Organ Tech Rep Ser 2012;v-xii:1–100.
19. Uttaro AD. Acquisition and biosynthesis of saturated and unsaturated fatty acids by trypanosomatids. Mol Biochem Parasitol 2014; 196:61–70.
20. de Macedo-Silva ST, de Souza W, Rodrigues JC. Sterol Biosynthesis Pathway as an Alternative for the Anti-Protozoan Parasite Chemotherapy. Curr Med Chem 2015;22:2186–2198.
21. Brun R. Schonenberger. Cultivation and in vitro cloning or procyclic culture forms of *Trypanosoma brucei* in a semi-defined medium. Short communication. Acta Trop 1979;36:289–292.
22. Coustou V, Biran M, Besteiro S, Riviere L, Baltz T, Franconi JM, Bringaud F. Fumarate is an essential intermediary metabolite produced by the procyclic *Trypanosoma brucei*. J Biol Chem 2006;281: 26832–26846.
23. Bringaud F, Baltz D, Baltz T. Functional and molecular characterization of a glycosomal PPi-dependent enzyme in trypanosomatids: pyruvate, phosphate dikinase. Proc Natl Acad Sci U S A 1998;95: 7963–7968.
24. Wirtz E, Leal S, Ochatt C, Cross GA. A tightly regulated inducible expression system for conditional gene knock-outs and dominant-negative genetics in *Trypanosoma brucei*. Mol Biochem Parasitol 1999;99:89–101.
25. Millerioux Y, Ebikeme C, Biran M, Morand P, Bouyssou G, Vincent IM, Mazet M, Riviere L, Franconi JM, Burchmore RJ, Moreau P, Barrett MP, Bringaud F. The threonine degradation pathway of the *Trypanosoma brucei* procyclic form: the main carbon source for lipid biosynthesis is under metabolic control. Mol Microbiol 2013;90: 114–129.
26. Deramchia K, Morand P, Biran M, Millerioux Y, Mazet M, Wargnies M, Franconi JM, Bringaud F. Contribution of pyruvate phosphate dikinase in the maintenance of the glycosomal ATP/ADP balance in the *Trypanosoma brucei* procyclic form. J Biol Chem 2014;289:17365–17378.
27. Riddles PW, Blakeley RL, Zerner B. Reassessment of Ellman's reagent. Methods Enzymol 1983;91:49–60.
28. Staack H, Binstock JF, Schulz H. Purification and properties of a pig heart thiolase with broad chain length specificity and comparison of thiolases from pig heart and *Escherichia coli*. J Biol Chem 1978;253:1827–1831.
29. Zeelen JP, Hiltunen JK, Ceska TA, Wierenga RK. Crystallization experiments with 2-enoyl-CoA hydratase, using an automated 'fast-screening' crystallization protocol. Acta Crystallogr D Biol Crystallogr 1994;50:443–447.
30. Adams PD, Afonine PV, Bunkoczi G, Chen VB, Davis IW, Echols N, Headd JJ, Hung LW, Kapral GJ, Grosse-Kunstleve RW, McCoy AJ, Moriarty NW, Oeffner R, Read RJ, Richardson DC, Richardson JS, Terwilliger TC, Zwart PH. PHENIX: a comprehensive Python-based system for macromolecular structure solution. Acta Crystallogr D Biol Crystallogr 2010;66:213–221.
31. Kabsch W. Xds. Acta Crystallogr D Biol Crystallogr 2010;66: 125–132.
32. Winn MD, Ballard CC, Cowtan KD, Dodson EJ, Emsley P, Evans PR, Keegan RM, Krissinel EB, Leslie AG, McCoy A, McNicholas SJ, Murshudov GN, Pannu NS, Potterton EA, Powell HR, Read RJ, Vagin A, Wilson KS. Overview of the CCP4 suite and current developments. Acta Crystallogr D Biol Crystallogr 2011;67: 235–242.
33. McCoy AJ, Grosse-Kunstleve RW, Adams PD, Winn MD, Storoni LC, Read RJ. Phaser crystallographic software. J Appl Crystallogr 2007;40:658–674.
34. Cowtan K. Completion of autobuilt protein models using a database of protein fragments. Acta Crystallogr D Biol Crystallogr 2012; 68:328–335.
35. Emsley P, Lohkamp B, Scott WG, Cowtan K. Features and development of Coot. Acta Crystallogr D Biol Crystallogr 2010;66:486–501.
36. Murshudov GN, Vagin AA, Dodson EJ. Refinement of macromolecular structures by the maximum-likelihood method. Acta Crystallogr D Biol Crystallogr 1997;53:240–255.
37. Modis Y, Wierenga RK. Crystallographic analysis of the reaction pathway of *Zoogloea ramigera* biosynthetic thiolase. J Mol Biol 2000; 297:1171–1182.
38. Kursula P, Ojala J, Lambeir AM, Wierenga RK. The catalytic cycle of biosynthetic thiolase: a conformational journey of an acetyl group through four binding modes and two oxyanion holes. Biochemistry 2002;41:15543–15556.
39. Krissinel E, Henrick K. Secondary-structure matching (SSM), a new tool for fast protein structure alignment in three dimensions. Acta Crystallogr D Biol Crystallogr 2004;60:2256–2268.
40. Chen VB, Arendall WB, 3rd, Headd JJ, Keedy DA, Immormino RM, Kapral GJ, Murray LW, Richardson JS, Richardson DC. MolProbity: all-atom structure validation for macromolecular crystallography. Acta Crystallogr D Biol Crystallogr 2010;66:12–21.
41. Krissinel E, Henrick K. Inference of macromolecular assemblies from crystalline state. J Mol Biol 2007;372:774–797.
42. Tamura K, Peterson D, Peterson N, Stecher G, Nei M, Kumar S. MEGA5: molecular evolutionary genetics analysis using maximum likelihood, evolutionary distance, and maximum parsimony methods. Mol. Biol Evol 2011;28:2731–2739.
43. Mazet M, Harijan RK, Kiema TR, Haapalainen AM, Morand P, Morales J, Bringaud F, Wierenga RK, Michels PA. The characterization and evolutionary relationships of a trypanosomal thiolase. Int J Parasitol 2011;41:1273–1283.
44. Riviere L, van Weelden SW, Glass P, Vegh P, Coustou V, Biran M, van Hellemond JJ, Bringaud F, Tielens AG, Boshart M. Acetyl:succinate CoA-transferase in procyclic *Trypanosoma brucei*. Gene identification and role in carbohydrate metabolism. J Biol Chem 2004;279: 45337–45346.
45. Millerioux Y, Morand P, Biran M, Mazet M, Moreau P, Wargnies M, Ebikeme C, Deramchia K, Gales L, Portais JC, Boshart M, Franconi JM, Bringaud F. ATP synthesis-coupled and -uncoupled acetate production from acetyl-CoA by mitochondrial acetate:succinate CoA-transferase and acetyl-CoA thioesterase in *Trypanosoma*. J Biol Chem 2012;287:17186–17197.
46. Froese DS, Forouhar F, Tran TH, Vollmar M, Kim YS, Lew S, Neely H, Seetharaman J, Shen Y, Xiao R, Acton TB, Everett JK, Cannone G, Puranik S, Savitsky P, Krojer T, Pilka ES, Kiyani W, Lee WH, Marsden BD, von Delft F, Allerston CK, Spagnolo L, Gileadi O, Montelione GT, Oppermann U, Yue WW, Tong L. Crystal structures of malonyl-coenzyme A decarboxylase provide insights into its catalytic mechanism and disease-causing mutations. Structure 2013;21: 1182–1192.
47. Bunkoczi G, Misquitta S, Wu X, Lee WH, Rojkova A, Kochan G, Kavanagh KL, Oppermann U, Smith S. Structural basis for different specificities of acyltransferases associated with the human cytosolic and mitochondrial fatty acid synthases. Chem Biol 2009;16:667–675.
48. Antonenkov VD, Van Veldhoven PP, Waelkens E, Mannaerts GP. Substrate specificities of 3-oxoacyl-CoA thiolase A and sterol carrier protein 2/3-oxoacyl-CoA thiolase purified from normal rat liver peroxisomes. Sterol carrier protein 2/3-oxoacyl-CoA thiolase is involved in the metabolism of 2-methyl-branched fatty acids and bile acid intermediates. J Biol Chem 1997;272:26023–26031.
49. Corey EJ, Sneen RA. Stereoelectronic Control in Enolization-Ketonization Reactions1. J Am Chem Soc 1956;78:6269–6278.
50. Panigrahi AK, Ogata Y, Zikova A, Anupama A, Dalley RA, Acestor N, Myler PJ, Stuart KD. A comprehensive analysis of *Trypanosoma brucei* mitochondrial proteome. Proteomics 2009;9:434–450.

51. Oefner C, Schulz H, D'Arcy A, Dale GE. Mapping the active site of Escherichia coli malonyl-CoA-acyl carrier protein transacylase (FabD) by protein crystallography. Acta Crystallogr D Biol Crystallogr 2006;62:613–618.
52. Zhang L, Liu W, Xiao J, Hu T, Chen J, Chen K, Jiang H, Shen X. Malonyl-CoA: acyl carrier protein transacylase from *Helicobacter pylori*: Crystal structure and its interaction with acyl carrier protein. Protein Sci 2007;16:1184–1192.
53. Serre L, Verbree EC, Dauter Z, Stuitje AR, Derewenda ZS. The Escherichia coli malonyl-CoA:acyl carrier protein transacylase at 1.5-A resolution. Crystal structure of a fatty acid synthase component. J Biol Chem 1995;270:12961–12964.
54. Liu Y, Feng Y, Wang Y, Li X, Cao X, Xue S. Structural and biochemical characterization of MCAT from photosynthetic microorganism Synechocystis sp. PCC 6803 reveal its stepwise catalytic mechanism. Biochem Biophys Res Commun 2015;457:398–403.
55. Franklin MC, Cheung J, Rudolph MJ, Burshteyn F, Cassidy M, Gary E, Hillerich B, Yao ZK, Carlier PR, Totrov M, Love JD. Structural genomics for drug design against the pathogen *Coxiella burnetii*. Proteins 2015;83:2124–2136.
56. Zhang L, Joshi AK, Smith S. Cloning, expression, characterization, and interaction of two components of a human mitochondrial fatty acid synthase. Malonyl transferase and acyl carrier protein. J Biol Chem 2003;278:40067–40074.
57. Rangan VS, Witkowski A, Smith S. Isolation of a functional transferase component from the rat fatty acid synthase by limited trypsinization of the subunit monomer. Formation of a stable functional complex between transferase and acyl carrier protein domains. J Biol Chem 1991;266:19180–19185.
58. Bretschneider T, Zocher G, Unger M, Scherlach K, Stehle T, Hertweck C. A ketosynthase homolog uses malonyl units to form esters in cervimycin biosynthesis. Nat Chem Biol 2011;8:154–161.
59. Stephens JL, Lee SH, Paul KS, Englund PT. Mitochondrial fatty acid synthesis in *Trypanosoma brucei*. J Biol Chem 2007;282:4427–4436.
60. Lee SH, Stephens JL, Englund PT. A fatty-acid synthesis mechanism specialized for parasitism. Nat Rev Microbiol 2007;5:287–297.